A nitrogen-responsive cytokinin oxidase/dehydrogenase regulates root response to high ammonium in rice

Lun Li[1], Letian Jia[1], Xingliang Duan[1], Yuanda Lv[2,3], Chengyu Ye[1], Chengqiang Ding[4,5,6], Yuwen Zhang[1], Weicong Qi[2,3], Hans Motte[7,8], Tom Beeckman[7,8], Le Luo[1*], Wei Xuan[1*]

[1]Sanya Institute of Nanjing Agricultural University, National Key Laboratory of Crop Genetics & Germplasm Enhancement and Utilization and MOA Key Laboratory of Plant Nutrition and Fertilization in Lower-Middle Reaches of the Yangtze River, Nanjing Agricultural University, Nanjing 210095, China

[2]Zhongshan Biological Breeding Laboratory, Nanjing 210014, China

[3]Excellence and Innovation Center, Jiangsu Academy of Agricultural Sciences, Nanjing 210014, China

[4]College of Agriculture, Nanjing Agricultural University, Nanjing 210095, China

[5]Key Laboratory of Crop Physiology Ecology and Production Management, Ministry of Agriculture, Nanjing 210095, China.

[6]Collaborative Innovation Center for Modern Crop Production co-sponsored by Province and Ministry, Nanjing 210095, China.

[7]Department of Plant Biotechnology and Bioinformatics, Ghent University, Technologiepark 71, B-9052 Ghent, Belgium

[8] Center for Plant Systems Biology, VIB, Technologiepark 71, B-9052 Ghent, Belgium

[*]Author for correspondence: Wei Xuan Email: wexua@njau.edu.cn; Le Luo Email: luole@njau.edu.cn

Summary

- Plant root system is significantly influenced by high soil levels of ammonium nitrogen, leading to reduced root elongation and enhanced lateral root branching. In *Arabidopsis*, these processes have been reported to be mediated by phytohormones and their downstream signaling pathways, while the controlling mechanisms remain elusive in crops.
- Through a transcriptome analysis of roots subjected to high/low ammonium treatments, we identified a cytokinin oxidase/dehydrogenase encoding gene, *CKX3*, whose expression is induced by high ammonium. Knocking out *CKX3* and its homologue *CKX8* results in shorter seminal roots, fewer lateral roots, and reduced sensitivity to high ammonium.
- Endogenous cytokinin levels are elevated by high ammonium or in *ckx3* mutants. Cytokinin application results in shorter seminal roots and fewer lateral roots in WT, mimicking the root responses of *ckx3* mutants to high ammonium. Furthermore, *CKX3* is transcriptionally activated by type-B RR25 and RR26, and *ckx3* mutants have reduced auxin content and signaling in roots under low ammonium.
- This study identified RR25/26-CKX3-cytokinin as a signal module that mediates root responses to external ammonium by modulating of auxin signaling in the root meristem and lateral root primordium. This highlights the critical role of cytokinin metabolism in regulating rice root development in response to ammonium.

Key Words: ammonium, auxin, CKX, cytokinin, lateral root, rice, seminal root

Introduction

The plant root system plays a pivotal role in sensing and absorbing water and nutrients from the soil. It primarily consists of the primary/seminal root, lateral roots (LRs), and root hairs, and their development are significantly influenced by external availability of nitrogen (N), which is one of the most essential macronutrients for plant physiological and developmental processes (Giehl & von Wirén, 2014; Motte, H. *et al.*, 2019). Two major N sources, ammonium (NH_4^+) and nitrate (NO_3^-), are not homogenously distributed in the soil due to their respective peculiarities regarding solubility and mobility (Xu *et al.*, 2012). Fluctuations in their soil concentration over space and time, referred to as "local N regimes", can trigger architectural changes in the plant root system. Such changes include the modulation of root elongation and root growth angle, the degree of root branching and the formation of root hairs (O'Brien *et al.*, 2016; Motte, Hans *et al.*, 2019). In the model plant *Arabidopsis*, a large number of molecules, including phytohormones, transporters, transcription factors, kinases and peptidases, have been identified to act as local or systemic signals that cooperatively regulate root development in response to external N regimes (Bellegarde *et al.*, 2017; Xuan *et al.*, 2017). Notably, NO_3^- and NH_4^+ supplies have an opposite impact on root growth. High NO_3^- levels positively regulate root growth, evidenced by the promotion of root elongation and LR emergence. However, exposure to high NH_4^+ strongly alters plant root system architecture, characterized by a shorter primary root and a reduced number of LRs (Qin *et al.*, 2008; Barth *et al.*, 2010; Li *et al.*, 2010). The inhibition of root growth by NH_4^+ is considered a significant symptom of NH_4^+ toxicity, and restricts the capacity of roots to forage nutrients and water from deeper soil layers (Britto & Kronzucker, 2002) .

The inhibitory effects of high NH_4^+ on rice root elongation has been observed in comparison with nitrate supply, has been documented in several studies (Hirano *et al.*, 2008; Xuan *et al.*, 2012; Xu *et al.*, 2013; Jia *et al.*, 2020), and the molecular mechanism governing root responses to NH_4^+ are of great concern (Li *et al.*, 2014; Liu *et al.*, 2020). In model plant *Arabidopsis*, the inhibition of NH_4^+ on root growth involves multiple biological pathways, including root apoplast acidification (Meier *et al.*, 2020) iron deposition in phloem (Liu, XX *et al.*, 2022), GDP-mannose and vitamin B_6 metabolism(Qin *et al.*, 2008; Barth *et al.*, 2010; Li *et al.*, 2010; Liu, Y *et al.*, 2022), and auxin transport (Li *et al.*, 2011). In crop rice, the NH_4^+ regulation of root development has been suggested to be associated with NH_4^+ uptake-induced root cell acidification (Jia *et al.*, 2020; Luo *et al.*, 2022), in which glutamine and arginine metabolism are involved (Hachiya *et al.*, 2021; Xie *et al.*, 2023), as well as the metabolism and signaling pathways of phytohormones (e.g. auxin, ethylene, brassinosteroid, and ABA) (Di *et al.*, 2018; Sun *et al.*, 2020; Li *et al.*, 2022; Wu *et al.*, 2022). Interestingly, phytohormones like auxin and cytokinin have been suggested to participate in the downstream regulation of NH_4^+ uptake and metabolism, mediating root growth responses to external high NH_4^+.

The phytohormone cytokinin (CK) has been demonstrated to mediate root development responses to external N conditions in *Arabidopsis* (Ruffel *et al.*, 2011; Ahmad *et al.*, 2023). Natural CKs include isopentenyl adenine (iP), *trans*-zeatin (tZ), *cis*-zeatin (cZ), and their conjugates (Kurakawa *et al.*, 2007). CK biosynthesis is catalyzed by the key enzymes isopentenyltransferase (IPT), cytochrome P450 monooxygenase CYP735A, and LONELY GUY (LOG), and CKs can be degraded by cytokinin oxidase/dehydrogenase (CKXs) (Tsai, Y-C *et al.*, 2012). Studies in *Arabidopsis* have shown that CK

responses and endogenous levels of CKs (Patterson *et al.*, 2010), especially of tZ, are specifically induced under high NO_3^- supply. tZ can act as a root-to-shoot mobile signal to activate systemic NO_3^- signaling, N uptake, and root development (Poitout *et al.*, 2018). This long-distance translocation of tZ between root and shoot is mediated by its transporter ATP-BINDING CASSETTE G SUBFAMILY 14 (ABCG14), and its knock-out disrupts tZ-induced root responses and the expression of the high-affinity NO_3^- transporter gene *NRT2.1* (Ko *et al.*, 2014; Zhang *et al.*, 2014). CKs have been shown to regulate rice root development through interacting with other phytohormones. For instance, CK signaling mutants of *Histidine Kinase 1* and *Authentic Histidine Phosphotransfer Protein 1/2* can alleviate the inhibition of root elongation by ethylene (Zhao *et al.*, 2020), and *hk1* mutants exhibit reduced root circumnutation (Taylor *et al.*, 2021). The cytokinin oxidase/dehydrogenase encoding gene *CKX4*, is transcriptionally activated by Auxin Response Factor 25 (ARF25) to promote rice crown root formation (Gao *et al.*, 2014). CKXs degrade CKs, thereby modulating CK homeostasis, and are typically induced by high CK levels (Frebort *et al.*, 2011). In rice, the *CKX* encoding gene family comprises 11 members, exhibiting differential expression patterns and functions in rice root tissues (Rong *et al.*, 2022). However, little is known about the role of CKXs in regulating root response to external N.

In this study, *CKX3* was identified to be transcriptional upregulated by NH_4^+ in rice roots. In roots, *CKX3*, together with its homologue *CKX8*, synergistically regulates the responses of both LR formation and seminal root elongation to external NH_4^+ supply through the manipulation of endogenous levels of CK and auxin signaling. Our results further reveal that *CKX3* is transcriptionally activated by the B-type CK response regulators RR25 and RR26, thus corroborating the existence of a RR25/26-CKX3-CK signaling module that mediates the NH_4^+ regulation of root development in rice.

Materials and Methods

Plant materials and growth conditions

Two rice cultivars, *Oryza sativa* L. ssp. *japonica* cv Nipponbare (NIP) and Wuyunjing7 (WYJ7), were used as wild-type lines in this study.The *DR5rev:3xVENUS-N7* transgenic reporter line was generated in the WYJ7 background and has been described previously (Yang *et al.*, 2017).

Rice seeds were soaked in 70% (v/v) ethanol for 2 min, then transferred into 50 ml 30% (v/v) sodium hypochlorite solution with a drop of Tween-80 (Product No. 9005-65-6, Yuanye Bio) for 30 min. After five times washing with fresh water, seeds were submerged in fresh water at 37 °C in the dark for 3 days. Germinated seeds were then grown in hydroponic cultures supplied with modified Kimura B solution under long day conditions (14 h photoperiod, 70% humidity, 28 °C) (Jia *et al.*, 2020). $(NH_4)_2SO_4$ was used as nitrogen donor, and 0.25 mM or 2.5 mM NH_4^+ were used as low N (LN) or high N (HN) treatment, respectively. During treatments, rice seedlings were grown for 7 days unless otherwise noted, and the nutrient solution was refreshed every 2 days.

Chemical treatments

6-BA (6-Benzyl adenine) (Product No. 1214-39-7) and iP (N^6-isopentenyladenine) (Product No. 2365-40-4) were purchased from Sigma-Aldrich (Shanghai, China). All chemicals were dissolved in 100% DMSO to make a 50 mM stock solution. To analyze the effect of 6-BA or iP on the phenotype, the germinated rice seedlings were grown under LN and HN conditions, in the presence or absence of 6-BA and iP at indicated concentrations for 7 days.

Plasmid construction and plant transformation

Knock-out single or double mutants of *CKX3*, *CKX8*, *RR25* and *RR26* were generated by using CRISPR/Cas9 genome editing technique (Miao *et al.*, 2013). Spacers residing in exons of the genes were selected from the website CRISPR-GE (http://skl.scau.edu.cn/), and cloned into single guide RNA expression cassettes by overlapping PCR. The obtained PCR fragments were subsequentially cloned into the BsaI site of the *pYLCRISPR–Cas9-MH* vector. To generate the overexpression line of *CKX3*, the *UBIL* promoter and *NOS* terminator were subcloned into the vector *pTCK303*, and the full-length CDS sequence of *CKX3* was amplified from the NIP cDNA and then ligated to *pTCK303* vector. To generate the transcriptional reporter line of *CKX3*, the 2043 bp DNA fragment upstream of *CKX3* start codon was amplified from NIP genomic DNA and cloned into *pCAMBIA1300*, while the *GUSPlus* gene and *NOS* terminator were subcloned into the vector *pCAMBIA1300*. For the construction of *Two Component signaling Sensor new* (*TCSn):GUS* vector, the Gateway cloning system (Invitrogen) was employed. *TCSn* sequence (Zurcher *et al.*, 2013) was first synthesized by Sangon biotech company, cloned into *pDONRP41R* using BP Clonase™ II, and then subcloned into the expression vector *pHb7m24GW*. All plasmids were transformed into rice plants using Agrobacterium-mediated transformation (Krishnan *et al.*, 2013). The primers used here are listed in Table **S1**.

Quantification of seminal root length and lateral root density

To quantify the root phenotype in NIP and indicated mutants, the emerged lateral roots produced along

the longest seminal root of indicated rice seedlings ($n \geq 10$) were counted under a microscope (Olympus SZ61). Subsequently, whole roots of rice seedlings were scanned using the Epson scanner Expression 11000XL at 600 dpi, and seminal root length was determined using Fiji image analysis software (http://fiji.sc/). Lateral root density was calculated by dividing the number of lateral roots by the length of the longest seminal root of each seedling. Relative seminal root elongation and lateral root density was normalized to WT under LN condition.

Transcriptome analysis

Sterilized NIP seeds were germinated in water under long day condition (14 h photoperiod, 70% humidity, 28 °C) for 3 days, and then transferred to hydroponic cultures supplied with modified Kimura B solution containing 0.125 mM or 1.25 mM $(NH_4)_2SO_4$ for 6 h and 24 h. At each time point, the root tip segments (~1 cm), comprising root meristem zone and elongation zone, from 40 NIP seedlings were excised and collected as one biological repeat. Three independent biological repeats were used for transcriptome analysis. RNA extraction and library construction was carried out by Novogene Bioinformatics Institute (Novogene Bioinformatics Technology, Beijing, China). Gene expression abundance was quantified by FPKM (Fragments Per Kilobase per Million) value. Differential expression was calculated via DEseq2 and genes were considered as differentially expressed genes (DEGs) with p-value < 0.05 (Table **S2**). Enrichment analysis based on Gene Ontology and KEGG databases was carried out using PlantGSAD (Ma *et al.*, 2022). Heatmap was plotted by custom R script.

qRT-PCR

Total RNA was isolated from the root tips of 4-day-old seedlings (≥3 individual seedlings per sample) by using TRIzol reagent (Product No. 10296–028, Thermo Fisher). RNA concentration and quantity were determined using Nanodrop 2000 (Thermo Fischer). A PrimeScript™ RT reagent Kit with gDNA Eraser (TaKaRa) was used to purify 1 μg total RNA and synthesize cDNA. Quantitative PCR (qPCR) was performed using the TB Green Premix Ex Taq™ (TaKaRa) on a LightCycler 480 Real-Time PCR system (Roche), according to the manufacturer's instructions. Melting curves were analyzed to check primer specificity. Normalization was done against the average of the reference genes *OsACTIN1* (LOC_Os03g50885) and *OsUbiquitin* (LOC_Os03g13170) with the $2^{-\Delta\Delta Ct}$ method. Each experiment was represented by at least three biological replicates. The primers used for the quantitative real-time PCR analyses are listed in Table **S3**.

Histochemical analysis

For the histochemical GUS assays, the roots of *pCKX3:GUS* and *TCSn:GUS* transgenic seedlings were collected and soaked in 90% acetone overnight, then transferred to 100 mM Tris/NaCl buffer (pH 7). After incubation at 37 °C for 30 min, the root tissues were soaked in Tris/NaCl buffer containing 2 mM X-gluc (Product No. 114162-64-0, Warbio), and 2 mM ferricyanide, and kept at 37 °C for 12 h. Samples were imaged with a Leica DM2500 microscope (Leica Microsystems). For anatomical sections, GUS-stained samples were fixed overnight and embedded following a published protocol (De Smet *et al.*, 2004). Transverse cutting was performed and further analyzed and captured using a Leica DM2500

microscope.

Subcellular localization

To determine the subcellular localization of CKX3, the genomic sequence of *CKX3* was amplified and fused in frame to GFP at either N- or C-terminus, and then the sequences were introduced into a *pBluescript* vector harboring the *35S* promoter. The resulted vectors containing *35S:CKX3-GFP* or *35S:GFP-CKX3* were co-transformed with the ER marker *35S:RFP-HDEL* into rice protoplasts for fluorescence observation using a Leica TCS SP8 X confocal laser scanning microscope. The rice protoplasts were isolated from 7-day-old seedlings according to a previous published method (He *et al.*, 2016) and 10 μg of each plasmid DNA was used for protoplast transformation by the polyethylene glycol method. The primers used here are listed in Table **S1**.

Confocal microscopy and quantification

To visualization the *DR5rev:3xVENUS-N7* signal in root tissues, the root of seedlings harboring *DR5rev:3xVENUS-N7* were cleared using a modified ClearSee method (Kurihara *et al.*, 2015). Root tissues were first fixed with 4% paraformaldehyde (Product No. 30525-89-4, Sigma-Aldrich) in PBS buffer under vacuum for 4 h at room temperature, washed twice with PBS, and then transferred to ClearSee solution for 4 days at room temperature. The *DR5rev:3xVENUS-N7* signal in root tissues was detected by Leica TCS SP8 X confocal laser scanning microscope. The quantifications of the fluorescence signal intensity in lateral root primordia and indicated tissue layers in the root tip were performed on individual seedlings.

Quantification of cytokinin derivates and auxin contents

To determine the contents of auxin and cytokinin derivates in roots, the germinated WT, *ckx3-1*, *ckx8-1*, *ckx3-1ckx8-1* and *rr25-1rr26-1* seedlings grown under LN and HN conditions for 7 days before used for measurement. Approximately 0.6 g of fresh seminal roots of 15 seedlings was excised and collected as one biological repeat. Fresh root tissues were immediately frozen in liquid nitrogen and ground into a powder. 0.05 g of powder was weighed and immediately transferred to a 1.5 mL centrifuge tube containing 1 mL of methanol/water/formic acid (15:4:1, v/v/v) extract and 10 μL the internal standard (100 ng/mL). The mixture was vortexed for 10 min and centrifuged at 10,000 g for 5 min at 4 °C, and then the supernatant was transferred into a new centrifuge tube. The solvent mixture was then concentrated in a stream of nitrogen gas, and the resulting sample was redissolved in 0.1 mL of 80% methanol and sonicated on ice for 5 min. After centrifuging at 10,000 g for another 15 min at 4 °C, the supernatant was filtered through a 0.22 μm organic membrane filter. The filtered solution was subsequently injected into a vial for LC-MS analysis. The standard solution is prepared and measured to construct a standard curve. Data acquisition was performed using Analyst 1.6.3 software (AB Sciex). All metabolites were quantified using Multiquant 3.0.3 software (AB Sciex). Three biological replicates were applied for quantification.

Yeast one-hybrid assay

Y1H assay was performed using the Matchmaker® Gold Yeast One Hybrid Library Screening System Kit (Clontech Biotechnology). The full-length coding sequences of *RR25* and *RR26* were cloned into the *pGADT7* vector, whereas the 2500 bp promoter of *CKX3* was clone into *pAbAi* vector. The above constructs were linearized and transformed into Y1HGold yeast strain as the bait reporter strain. Then, the yeast expression vector with empty vector or the coding sequences of *RR25* and *RR26* were respectively transformed into the bait reporter strain for Aureobasidin A (AbA) screening. The primers used to construct the vectors are listed in Table **S1**.

Transient transactivation assay

Leaf protoplasts were extracted from two-week-old rice seedling for transient transactivation assay. The full-length coding sequences of *RR25* and *RR26* were cloned into the *PB7WG-2.0* vector to generate the effectors. The 2.5 kb promoter of *CKX3* was amplified and fused to the firefly luciferase (LUC), and introduced into the *pGreen-II 0800* vector. Plasmids containing the effector and reporter vectors were transfected into rice protoplasts. The untransfected protoplasts (water only) and protoplasts transfected with the reporter vector only (empty vector) were used as negative controls. The protoplast proteins were extracted, and the renilla luciferase (REN) or LUC activities were detected by using the Dual-luciferase® reporter assay system (Product No.E1910,Promega) after 16 h infiltration under light or dark conditions. Three-leaf stage tobacco (ssp. *Nicotiana benthamiana*) grown in a plant growth incubators were used for transient transactivation assays as previously described (Hellens *et al.*, 2005). The effector and reporter vector were co-transformed via Agrobacterium-mediated transformation into tobacco leaves. Leaves transiently transformed with only the reporter vector were used as a negative control. The activities were measured by using LUC dye (iKon-M from Andor, Model No, DU934P-BV) in the dark and photographed under a fluorescent camera after incubation in the dark for 3 days. The primers used to construct the vectors are listed in Table **S1**.

Statistical analysis

The experimental data were obtained from at least three independent biological repeats. Statistical analyses were done using GraphPad Prism 8 software. The significant difference among sets of data was determined by student's two-tailed t-test ($p < 0.05$), while significant differences among multiple data sets were used by one-way ANOVA and Duncan's multiple comparison.

Results

Transcriptome analysis identifies *CKX3* as a high N responsive gene.

To explore the molecular components that regulate the root responses to high NH_4^+, we performed global transcriptional comparisons on the root tissues of rice wild-type (WT) seedlings grown under low N (LN, 0.25 mM NH_4^+) and high N (HN, 2.5 mM NH_4^+) conditions for respectively 6 hours and 24 hours (Fig. **1a**). In total, 4327 differentially expressed genes (DEGs) and 3413 DEGs (p-value < 0.05) were identified after 6 hours and 24 hours treatments, respectively (Fig. **1b** and **S1a**, Table **S2**). Among which, 1470 DEGs showed differentially expression under both time points under HN treatment (Fig. **1b**). We next performed KEGG and Gene Ontology (GO) enrichment of DEGs to gain insights into their potential involvement in various biological pathways under HN and LN conditions (Fig. **1c**). KEGG analysis showed that these co-regulated DEGs by HN supply are predicted to be involved in pathways related to N metabolism, biosynthesis of secondary metabolites and amino acid biosynthesis (Fig. **S1b**). The GO enrichment analysis indicated that HN treatment causes interferes strongly with diverse biological processes, including N assimilation, amino acid transmembrane transport, ethylene signaling pathway, ion transmembrane transport and carbohydrate metabolic processes (Fig. **1c**), in line with the dominant effects of NH_4^+ on rice root development and physiology.

Of particular interest, our transcriptome data suggest a potential effect on cytokinin dehydrogenase (CKX) activity by the NH_4^+ condition in the root (Fig. **1c**) because the CKX encoding genes, *CKX3* and *CKX8*, were transcriptional induced after HN treatment for 6 h and 24 h, while the expression levels of *CKX4* and *CKX5* were reduced after 6 h HN treatment (Fig.**1d**). qRT-PCR analysis confirmed the induction of *CKX3* and *CKX8* expressions in roots by HN after 24 hours treatment, while the induction on *CKX3* expression was more pronounced (Fig. **2a**). Further time-lapse analysis showed that the induction of *CKX3* expression by HN was evident after 2 hours treatment, and reached its peak level at 12 hours (Fig. **2b**).

To visualize the tissue-specific expression pattern of *CKX3* in roots, we generated a transcriptional reporter line by fusing the GUS reporter gene to its native promoter (*CKX3pro:GUS*). GUS staining of *CKX3pro:GUS* transgenic seedlings revealed strong promoter activity in the root cap and in phloem cells in the elongation and differentiation zones, but not in the meristematic zone (Fig. **2c,d**, and **S2**). Furthermore, the expression level was induced by high NH_4^+ (Fig. **2c,d**) supporting the idea that *CKX3* is a NH_4^+-responsive gene in rice roots. At the protein level, CKX3 is localized to the endoplasmic reticulum (ER), as indicated by its co-localization with the ER marker HDEL (Meng *et al.*, 2022) (Fig. **S3**).

CKX3 mediates root elongation and lateral root formation in response to NH_4^+

To investigate the role of CKX3 in regulating rice root responses to NH_4^+, we generated knock-out mutants and overexpression lines of *CKX3*, and analyzed their root phenotypes under different NH_4^+ conditions. Three knock-out mutants of *CKX3*, *ckx3-1*, *ckx3-2*, *and ckx3-3*, were generated using the CRISPR-Cas9 genome editing technique (Fig. **S4a**). Two overexpression lines of *CKX3*, *OE #1* and *OE #2*, were constructed under the control of ubiquitin promoters and showed increased expression of *CKX3* in the root (Fig. **S4b**). We found that WT seedlings displayed shorter seminal roots but increased LR

density under HN conditions compared to LN conditions (Fig. **3a-c**). In three mutants of *CKX3*, seminal root elongation and LR formation were both suppressed under either HN or LN condition (Fig. **3a**). Remarkably, the root sensitivity to external NH_4^+ was less pronounced in the three *CKX3* mutant lines compared to WT, as evidenced by similar LR density and smaller differences on seminal root elongation observed between HN- and LN-treated *CKX3* mutants (Fig. **3b,c**). In addition, two *CKX3* overexpression lines showed no difference with WT on root growth under both either LN or HN condition (Fig. **S5a-c**).

We further compared the meristem length and cell number between WT and *ckx3* mutants under different N conditions. The *ckx3* mutants had reduced meristem length and cell number compared to WT under either LN or HN condition (Fig. **4a-c**). Importantly, both root meristem cell number and meristem length were significantly decreased in WT seedlings under HN condition, while this difference became smaller in three *CKX3* mutants (Fig. **4a-c**). This result is consistent with the observations that root elongation in *ckx3* is less sensitive to external N conditions (Fig. **3a,c**), and further indicates that the *CKX3*-mediated seminal root elongation under different N conditions is a result from cell division activity at root meristem.

CKX8 shares similar function with *CKX3* on regulating root responses to ammonium

Sequence analysis and homologous comparison showed that the amino acid sequence of CKX3 shares high identity (59.74 %) with another *CKX* family member, CKX8 (Fig. **S6**). Transcriptome analysis also indicated that, similar to *CKX3*, the expression level of *CKX8* in the root was induced by HN (Fig. **1d, 2a**). This suggests that *CKX8* shares a similar function with *CKX3* in regulating root development in response to NH_4^+.

To test our hypothesis, we generated a single mutant of *CKX8* (*ckx8-1*) and a double mutant of *CKX3* and *CKX8* (*ckx3-1ckx8-1*) using the CRISPR-Cas9 technique (Fig. **S4a**), and compared their root phenotypes with WT under different NH_4^+ conditions. Compared to WT, *ckx8-1* had shorter seminal root than WT under both LN or HN condition, and exhibited reduced sensitivity of seminal root elongation to external NH_4^+ compared to WT (Fig. **5a,c**). However, *ckx8-1* showed identical sensitivity of LR density to external NH_4^+ as WT (Fig. **5b**). In comparison to the single mutants of *CKX3* and *CKX8*, the double mutant *ckx3-1ckx8-1* exhibited enhanced inhibitory effects on both seminal root elongation and LR density under either LN or HN condition (Fig. **5a,c**). *ckx3-1ckx8-1* showed reduced sensitivity of LR density to external NH_4^+ than WT, while the insensitivity of seminal root elongation to NH_4^+ was more pronounced in *ckx3-1ckx8-1* than the single mutants (Fig. **5a-c**). These results suggest that *CKX3* and its homologue *CKX8* act together to regulate root development responses to external NH_4^+.

CKX3 and CKX8 modulate the CK homeostasis in root

The CK homeostasis depends on its biosynthesis and degradation *in vivo*. As CK biosynthesis is mediated by IPT, CYP35A, and LOG, the CK degradation of CK is regulated by CKXs (Schmülling *et al.*, 2003; Tsai, YC *et al.*, 2012; Kieber & Schaller, 2018). Transcriptome and RT-qPCR analysis showed that several IPT, CYP35A, and LOG family genes were up-regulated under HN condition, indicating the CK biosynthesis is activated by high NH_4^+ (Fig. **S7**). To investigate whether CKX3 and CKX affect the endogenous CK homeostasis, we quantified the content of CKs and derivates, including iP, tZ, cZ, cZR,

and iPR, in the roots of WT, *ckx3-1*, *ckx8-1*, and *ckx3-1ckx8-1*under different NH_4^+ conditions. The CKs showed different abundances in the roots of WT and mutants upon different NH_4^+ conditions (Fig. **6a**). Under HN condition, the contents of tZ, iPR, and total CKs were increased in the WT root, in agree with higher expression of several CK biosynthesis genes. The content of iP was elevated in the roots of WT and all the mutants under LN condition; while its content was relative higher in *ckx3-1* and *ckx8-1* in relation to WT, and become more pronounced in *ckx3-1ckx8-1*. Higher contents of tZ, cZR, and iPR were detected in *ckx3-1*, *ckx8-1*, and *ckx3-1ckx8-1* than WT under HN condition, but there was no difference among WT, *ckx3-1*, *ckx8-1*, and *ckx3-1ckx8-1* under LN condition. In addition, the content of cZ was increased in *ckx3-1*, *ckx8-1*, and *ckx3-1ckx8-1* roots under both LN and HN conditions. The total content of CKs derivatives was significantly increased in WT and the mutants of *CKX3* and *CKX8* under HN condition, and *ckx3-1*, *ckx8-1*, and *ckx3-1ckx8-1* had higher content of total CK derivatives than WT under both LN and HN condition (Fig. **6a**).

To assess whether the increased content of CKs in *ckx3-1* provoked endogenous CK signaling in the root, we generated the CK responsive reporter line *TCSn:GUS* and introduced it into *ckx3-1*. The *TCSn:GUS* signal was strongly detected the in root cap and differentiation zone, but absent in the root meristem and elongation zone (Fig. **6b**). This is similar to its expression pattern in *Arabidopsis* (Chang *et al.*, 2019). Interestingly, there was no obvious difference in *TCSn:GUS* expression in the root tip regions of WT and *ckx3-1* under LN condition (Fig. **6b**). However, *TCSn:GUS* expression in roots was induced by HN, and *ckx3-1* roots showed stronger *TCSn:GUS* signal compared to WT under either LN or HN condition (Fig. **6b**). These results together suggest a crucial role of *CKX3* in regulating CK homeostasis in the root.

Cytokinin modulates the root responses to external NH_4^+

We subsequently examined whether the accumulation of CKs in *ckx3* is associated with CKX3-mediated root responses to external NH_4^+. To address this, *ckx3-1* and WT seedlings were treated with exogenous 6-BA and iP under both LN and HN conditions. Exogenous 6-BA and iP treatments caused notable reduction of seminal root elongation and completely blocked LR formation in WT and *ckx3-1* under both conditions (Fig. **7a,b**). The responsiveness of both seminal root elongation and LR formation to external NH_4^+ was abolished in both WT and *ckx3-1* when treated with 6-BA or iP (Fig. **7a,b**).

Furthermore, the application of exogenous 6-BA and iP induced the expression of *CKX3* and also *CKX8* in the root after 6 hours treatment (Fig. **7c**), showing that *CKX3* and *CKX8* are transcriptionally activated to degrade excess CKs *in vivo*. These results underscore the important role of CKX3 and CK homeostasis in regulating root development in response to NH_4^+.

***CKX3* expression is regulated by RRs**

It has been reported that B-type CK response regulators (RRs) are able to transcriptionally activate *CKXs*, thereby regulating rice root development (Gao *et al.*, 2014). Our transcriptome analysis showed that B-type RRs encoding genes *RR22*, *RR23*, and *RR26* were transcriptionally induced in the root of WT by HN after 6 hours treatment, and the induction became stronger after 24 hours treatment (Fig. **8a**). Among them, the expressions of *RR26* showed the highest induction by NH_4^+, mirroring the

transcriptional response of *CKX3* to NH_4^+ (Fig. **8a**). This data hints at a molecular link between the B-type RRs and CKX3.

The promoter region of *CKX3* contains five repeats of the putative RR binding element "AGATT" (Gao *et al.*, 2014) (Fig. **8b**). To investigate whether B-type RRs can directly bind to the promoter of *CKX3*, yeast-one-hybrid and transient transactivation experiments were conducted *in vitro*. Both tests showed that RR25 and RR26 could both bind to the promoter of *CKX3* and activated *CKX3* expression (Fig. **8c-e**). We further generated two double knock-out mutants of *RR25* and *RR26* (Fig. **S8**), and validated the expression level of *CKX3* in the roots of NIP and *rr25-1rr26-1* under both LN and HN condition. The results showed that HN treatment led to increased expression of *CKX3* in the roots of both NIP and *rr25-1rr26-1*, while the expression level of *CKX3* is lower in *rr25-1rr26-1* than in WT under both LN and HN conditions (Fig. **8f**). This result confirms that the expression of *CKX3* is positively regulated by RR25 and RR26.

We next compared the mutant root phenotypes with WT under different N conditions. *rr25rr26* double mutants showed slightly longer seminal root and higher LR density than WT under either LN or HN condition, while they showed identical sensitivities of seminal root elongation and LR formation to external NH_4^+ as WT (Fig. **8f,g**). Quantification of contents of IAA, IBA and CK derivatives also showed a higher level of cZ in *rr25-1rr26-1* than WT under both LN and HN condition, while there is no notable difference in the contents of IAA, IBA and total CKs between WT and *rr25-1rr26-1* (Fig. **S9**). Furthermore, exogenous 6-BA treatment could cause strong inhibition on the seminal root elongation and LR formation in *rr25-1rr26-1* under either LN or HN condition, mimicking its inhibitory effects on the root growth of WT (Fig. **S10**).

CKX3-mediated modulation of root responses to NH_4^+ involves auxin signaling

CK is known to act antagonistic with auxin to regulate root development (Aloni *et al.*, 2006; Ruzicka *et al.*, 2009; Su *et al.*, 2011; Kurepa & Smalle, 2022). However, it is unclear how auxin response is affected by CK at the tissue level under varying NH_4^+ supplies. To investigate this, we introduced the sensitive auxin-responsive reporter *DR5rev:3xVENUS-N7* into *ckx3-1* and quantified its expression pattern in different root tissues under different NH_4^+ conditions (Fig. **9a**). Consistent with our previous results (Xie *et al.*, 2023), the *DR5* signal was elevated in the root stele of WT seedlings under LN condition, while it was reduced in the root epidermal cells (Fig. **9a,b**). In *ckx3-1*, *DR5* signals in both stele and epidermal cells were substantially reduced under both LN or HN condition (Fig. **9a,b**). In a next experiment, we analyzed the effects of exogenous 6-BA and iP on *DR5* expression in WT and *ckx3-1* under different N conditions. iP or 6-BA largely suppressed the LN-induced *DR5* signal in root stele cells of WT seedlings (Fig. **9a,b**). However, both iP and 6-BA treatments led to the accumulation of *DR5* signal in the root epidermal cells of WT and *ckx3-1* seedlings regardless of external NH_4^+ supplies (Fig. **9a,b**). Considering the inhibitory effects of iP or 6-BA on root elongation, the increased CK level in *ckx3-1* may suppress root elongation by attenuating auxin signal in the stele, which is required for maintaining root elongation.

The expression pattern of *DR5* in the LR primordium was also analyzed. *DR5* expression in the LR primordia of WT was lower under HN conditions compared to LN conditions. Additionally, *DR5* expression in LR primordia was further reduced in *ckx3-1* under both HN and LN conditions (Fig. **10a,b**).

Moreover, iP and 6-BA treatments substantially reduced *DR5* expression in LR primordia of WT seedlings, resembling the *DR5* expression pattern in *ckx3-1* (Fig. **10a,b**). Hence, CKX3-mediated CK homeostasis might affect auxin signaling to regulate root responses to external NH_4^+.

Discussion

The root system architecture is a vital determinant of plant growth potential because its significant roles in nutrient uptake and stress avoidance (Rogers & Benfey, 2015; Khan *et al.*, 2016; Jia & von Wiren, 2020; Maqbool *et al.*, 2022). However, high NH_4^+ supply causes severe inhibition on plant root growth, limiting the root uptaking nutrient and water from deep soil. Understanding the regulatory mechanisms underlying and identification of regulators are of great agronomic importance. In this study, by performing a genome-wide transcriptome analysis of root tissues treated with or varied NH_4^+ concentrations we identified a high NH_4^+-responsive gene *CKX3* as a critical regulator in root development. It also acted in the process of root responses to high NH_4^+ through modulating endogenous CK homeostasis and auxin signaling (Fig. **11**).

In rice, CKX family comprises 11 members, which have divergence but redundancy function in rice shoot and root development (Rong *et al.*, 2022). For instance, *CKX2* did not express in root, and it inhibited tiller and grain numbers; CKX4 and CKX9 acted cooperatively to suppress tiller formation in rice (Ashikari, Motoyuki *et al.*, 2005; Yeh *et al.*, 2015; Duan *et al.*, 2019; Rong *et al.*, 2022). *CKX4* also exhibited strongly expression at rice root stele and the base of shoot where crown root initiated, and it positively regulates root elongation and crown root formation (Gao *et al.*, 2014); while CKX5 has been found to promote LR and crown root formation, and enhance nutrient uptake (Gao *et al.*, 2014; do Nascimento *et al.*, 2021). CKX3 has been previously reported to promote internode development, plant height and yield in rice (Rong *et al.*, 2022). A recent study also showed that CKX3 plays a negative role in leaf angle through regulating lamina joint development (Huang *et al.*, 2023). Our study uncovered the role of CKX3 in root development, and revealed that *CKX3* not merely regulates root elongation and LR formation, but also mediates their sensitivity to external NH_4^+. We showed that *CKX3* knock-out mutants had increased endogenous CK content and signaling in root (Fig. **6**), leading to short seminal root and decreased LR density under both LN and HN conditions (Fig. **3**). Whilst the decreased root growth in the mutants of *CKX3* was more pronounced under LN condition, mimicking the WT root phenotype under HN condition (Fig. **3**). High NH_4^+ supply led to increased CK content and signaling in WT root (Fig. **6**), and treatments of exogenous CK analogues also attenuated the seminal root elongation and LR formation (Fig. **6**). Our results thereby suggested that NH_4^+ inhibition on root development is probably due to the increased CK content, that is governed by CKXs.

Noticeably, both transcriptome and qPCR results revealed that the expression levels of *CKX4*, *CKX10*, and *CKX11*, were also induced by high NH_4^+ after 12 h (Fig. **1d**, **2a**), indicating that other CKX members might also play roles in modulating CK content and root development (Fig. **11**). Indeed, among them, *CKX8* is the closest homologue of *CKX3* with segmental duplication (Ashikari, M. *et al.*, 2005), and it exhibits similar function in regulating root development and its response to NH_4^+ (Fig. **5**). The double mutants of *CKX3* and *CKX8* had enhanced root growth defect phenotype under HN to LN conditions than either single mutant, with substantially reduction of root sensitivity to external NH_4^+ (Fig.

5). Thus, *CKX3* and *CKX8*, could act as a pair of N-responsive genes, to cooperatively mediate root response to external NH_4^+. Further study would also be interesting to generate knock-out mutants of other *CKX* gene members and investigate their roles in regulating root response to N.

CKXs mainly function on the biodegradation of CK derivatives, but they can target different CK derivates (Rong *et al.*, 2022). In *Arabidopsis*, CKX3 mainly acts on the metabolism of iP phosphates and iPR (Kowalska et al., 2010), while it targets tZ and iP in rice shoot (Huang *et al.*, 2023). Consistently, our results also showed that CKX3 is responsible for the degradation of iP and cZ in root under LN condition (Fig. **6a**); however, CKX3 was found to regulate the degradation of more CK derivates under high NH_4^+ condition, including tZ, cZR, iPR, whose contents were highly accumulated under high NH_4^+ condition (Fig. **6a**). This suggests that CKX3 could target different substrates depending on the changes of the endogenous level of CK derivates. Furthermore, treatment of iP, the major substrates of CKX3 under low NH_4^+ condition, could exacerbate the impaired root phenotype of *CKX3* mutant (Fig. **7**). Hence, the function of CKX3 in controlling iP homeostasis is required for maintaining root development under LN condition. In contrast, under HN condition, the contents of more types of CK derivates were accumulated in root (Fig. **6a**), thus other CKXs might also activated to modulate endogenous content of CK derivates under high NH_4^+ condition. Future experiments will generate higher-order mutant of CKX family members and investigate their roles in regulating CK homeostasis and root responses to external NH_4^+.

In *Arabidopsis*, CK has been demonstrated to regulate primary root and LR formation through antagonistic interaction with auxin signaling (Ruzicka *et al.*, 2009; Bishopp *et al.*, 2011). During LR formation, CK can repress auxin signaling at the early stage LR primordia to prevent LR formation (Laplaze *et al.*, 2007; Dubrovsky *et al.*, 2008). Our results also revealed that, under either low or high NH_4^+ condition, the auxin signaling can be strongly suppressed in seminal root and LR primordia in the mutants of *CKX3* or upon CK treatments (Fig. **9**, **10**), corresponding with reduced seminal root elongation and LR formation. Thus, the regulation of CKX and CK on rice root response to NH_4^+ is also mediated by auxin. Previous study also suggested that CKX4 acts downstream of transcription factors RR22, RR23, ARF25, and NAC4, which can bind the promoter of *CKX4* and modulates its expression (Gao *et al.*, 2014; Mao *et al.*, 2020). In this study, out results also identified two B-type RRs, RR25 and RR26, that can bind to the promoter of *CKX3* and positively regulates its expression. *RR26* also exhibited higher expression levels in root under HN condition. Although their mutants showed slightly longer seminal root and higher LR density than WT, they had no impact on root responses regarding varying NH_4^+ supplies, as well as endogenous auxin and CK levels (Fig. **S9**). This might be owing to the function redundancy of RR family members, and other uncharacterized transcription factors might also play roles in regulating *CKX3* transcription, which needs further investigation. A recent study in *Arabidopsis* has identified GRAS transcription factor SHORT-ROOT (SHR) as the upstream regulator of CKX3 during the regulation of CK homeostasis (Yang *et al.*, 2021). By specific screening for N-responsive transcription factors in our transcriptome dataset, we further identified 59 transcription factors, that are regulated by external N condition in root (Fig. **S11**). Among these N-responsive transcription factors, we further searched for the ones that might directly target the promoter of *CKX3*. Potential binding sites of DNA binding with One Finger (DOF), Basic helix-loop-helix (bHLH), basic leucine zipper (bZIP),

WRKY, and NIN-like protein (NLP) transcription factors were identified in the promoter region of *CKX3* (Fig. **S12**). These results indicate the expression of *CKX3* might be co-regulated by multiple N-responsive transcription factors (Fig. **11**).

In summary, our study uncovered a RR25/RR26-CKX3-CK signaling module transcriptionally regulated by NH_4^+, mediating the root growth responses to external NH_4^+ (Fig. **11**). CKX3 can modulate the homeostasis of endogenous CK derivates, especially iP, which metabolism determines the root growth under low NH_4^+ conditions through affecting auxin signaling. This study will facilitate our understanding of the molecular mechanism of root formation in cereal plants and may ultimately be helpful for root engineering in improving cereal crop root architecture and nutrient utilization.

Acknowledgements

We thank Hongye Qu and Xiaoli Dai for their technical help with confocal imaging. This work was supported by China National Key Program for Research and Development (2021YFF1000403), Zhongshan Biological Breeding Laboratory Project (KY2023-06 and BM2022008-03), the Fundamental Research Funds for the Central Universities (KYT2023001), National Natural Science Foundation (No. 32072658), Key Research and Development Program of Jiangsu Province (BE2020339), Jiangsu Seed Industry Revitalization Project (JBGS [2021] 011).

Competing interests

None declared.

Author contributions

WX and LeLuo: conceptualization; LunLi: performing the most of the experiments; LTJ; XLD and YDL: Assisted in the transcriptome data analysis; CYY and WCQ: performing preliminary analysis of the mutant phenotype; YWZ and CQD: constructing part of the CRISPR vectors; TB and HM commented on this work; LunLi, LeLuo and WX: data analysis and writing the article; all the authors discussed the results and contributed to the finalization of the manuscript.

Data availability

All the raw sequencing data have been deposited in the NCBI SRA database under BioProject accession PRJNA1150534. Gene accession in the study can be found in the GenBank/EMBL databases under the following accession numbers: *CKX1* (LOC_Os01g09260), *CKX2* (LOC_Os02g40710), *CKX3* (LOC_Os10g34230), *CKX4* (LOC_Os01g71310), *CKX5* (LOC_Os01g56810), *CKX7* (LOC_Os02g12780), *CKX8* (LOC_Os04g44230), *CKX9* (LOC_Os05g31040), *CKX10* (LOC_Os06g37500), *CKX11* (LOC_Os08g35860), *RR21* (LOC_Os03g12350), *RR22* (LOC_Os06g08440), *RR23* (LOC_Os02g55320), *RR24* (LOC_Os02g08500), *RR25* (LOC_Os06g43910), *RR26* (LOC_Os01g67770), *IPT4* (LOC_Os03g59570), *IPT7* (LOC_Os05g47840), *IPT8* (LOC_Os01g49390), *IPT9* (LOC_Os01g73760), *CYP735A3* (LOC_Os08g33300), *CYP735A4* (LOC_Os09g23820), *LOG* (LOC_Os01g40630), *LOGL1* (LOC_Os01g51210), *LOGL2* (LOC_Os02g41770), *LOGL3* (LOC_Os03g01880), *LOGL4* (LOC_Os03g49050), *LOGL5* (LOC_Os03g64070), *LOGL6* (LOC_Os04g43840), *LOGL7* (LOC_Os05g46360), *LOGL8* (LOC_Os05g51390), *LOGL9* (LOC_Os09g37540), *LOGL10* (LOC_Os10g33900), *Ubiquitin* (LOC_Os03g13170) and *ACTIN1* (LOC_Os03g50885).

References

Ahmad N, Jiang Z, Zhang L, Hussain I, Yang X. 2023. Insights on phytohormonal crosstalk in plant response to nitrogen stress: a focus on plant root growth and development. *International Journal of Molecular Sciences* **24**.

Aloni R, Aloni E, Langhans M, Ullrich CI. 2006. Role of cytokinin and auxin in shaping root architecture: regulating vascular differentiation, lateral root initiation, root apical dominance and root gravitropism. *Annals of Botany* **97**: 883-93.

Ashikari M, Sakakibara H, Lin S, Yamamoto T, Takashi T, Nishimura A, Angeles ER, Qian Q, Kitano H, Matsuoka M. 2005. Cytokinin oxidase regulates rice grain production. *Science* **309**: 741-5.

Barth C, Gouzd ZA, Steele HP, Imperio RM. 2010. A mutation in GDP-mannose pyrophosphorylase causes conditional hypersensitivity to ammonium, resulting in *Arabidopsis* root growth inhibition, altered ammonium metabolism, and hormone homeostasis. *Journal of Experimental Botany* **61**: 379-94.

Bellegarde F, Gojon A, Martin A. 2017. Signals and players in the transcriptional regulation of root responses by local and systemic N signaling in *Arabidopsis thaliana*. *Journal of Experimental Botany* **68**: 2553-65.

Bishopp A, Benkova E, Helariutta Y. 2011. Sending mixed messages: auxin-cytokinin crosstalk in roots. *Current Opinion in Plant Biology* **14**: 10-6.

Britto DT, Kronzucker HJ. 2002. NH_4^+ toxicity in higher plants: a critical review. *Journal of Plant Physiology* **159**: 567-84.

Chang J, Li X, Fu W, Wang J, Yong Y, Shi H, Ding Z, Kui H, Gou X, He K, et al. 2019. Asymmetric distribution of cytokinins determines root hydrotropism in *Arabidopsis thaliana*. *Cell Research* **29**: 984-93.

De Smet I, Chaerle P, Vanneste S, De Rycke R, Inzé D, Beeckman T. 2004. An easy and versatile embedding method for transverse sections. *Journal of Microscopy* **213**: 76-80.

Di D-W, Sun L, Zhang X, Li G, Kronzucker HJ, Shi W. 2018. Involvement of auxin in the regulation of ammonium tolerance in rice (*Oryza sativa* L.). *Plant and Soil* **432**: 373-87.

Do Nascimento FC, de Souza AFF, de Souza VM, Rangel RP, Zonta E, Fernandes MS, Santos LA. 2021. OsCKX5 modulates root system morphology and increases nutrient uptake in rice. *Journal of Plant Growth Regulation* **41**: 2157-70.

Duan J, Yu H, Yuan K, Liao Z, Meng X, Jing Y, Liu G, Chu J, Li J. 2019. Strigolactone promotes cytokinin degradation through transcriptional activation of CYTOKININ OXIDASE/DEHYDROGENASE 9 in rice. *Proceedings of the National Academy of Sciences*, *USA* **116**: 14319-24.

Dubrovsky JG, Sauer M, Napsucialy-Mendivil S, Ivanchenko MG, Friml J, Shishkova S, Celenza J, Benková E. 2008. Auxin acts as a local morphogenetic trigger to specify lateral root founder cells. *Proceedings of the National Academy of Sciences*, *USA* **105**: 8790-4.

Frebort I, Kowalska M, Hluska T, Frebortova J, Galuszka P. 2011. Evolution of cytokinin biosynthesis and degradation. *Journal of Experimental Botany* **62**: 2431-52.

Giehl RF, von Wirén N. 2014. Root nutrient foraging. *Plant Physiology* **166**: 509-17.

Gao S, Fang J, Xu F, Wang W, Sun X, Chu J, Cai B, Feng Y, Chu C. 2014. CYTOKININ OXIDASE/DEHYDROGENASE 4 integrates cytokinin and auxin signaling to control rice crown Root formation. *Plant Physiology* **165**: 1035-46.

Hachiya T, Inaba J, Wakazaki M, Sato M, Toyooka K, Miyagi A, Kawai-Yamada M, Sugiura D, Nakagawa T, Kiba T, et al. 2021. Excessive ammonium assimilation by plastidic glutamine synthetase causes ammonium toxicity in *Arabidopsis thaliana*. *Nature Communications* **12**: 4944.

He F, Chen S, Ning Y, Wang GL. 2016. Rice (*Oryza sativa*) protoplast isolation and its application for transient expression analysis. *Current Protocols in Plant Biology* **1**: 373-83.

Hellens RP, Allan AC, Friel EN, Bolitho K, Grafton K, Templeton MD, Karunairetnam S, Gleave AP, Laing WA. 2005. Transient expression vectors for functional genomics, quantification of promoter activity and RNA silencing in plants. *Plant Methods* **1**: 13.

Hirano T, Satoh Y, Ohki A, Takada R, Arai T, Michiyama H. 2008. Inhibition of ammonium assimilation restores elongation of seminal rice roots repressed by high levels of exogenous ammonium. *Physiologia Plantarum* **134**: 183-90.

Huang P, Zhao J, Hong J, Zhu B, Xia S, Zhu E, Han P, Zhang K. 2023. Cytokinins regulate rice lamina joint development and leaf angle. *Plant Physiology* **191**: 56-69.

Jia L, Xie Y, Wang Z, Luo L, Zhang C, Pelissier PM, Parizot B, Qi W, Zhang J, Hu Z, et al. 2020. Rice plants respond to ammonium stress by adopting a helical root growth pattern. *The Plant Journal* **104**: 1023-37.

Jia Z, Giehl RFH, von Wiren N. 2022. Nutrient-hormone relations: Driving root plasticity in plants. *Molecular Plant* **15**: 86-103.

Jia Z, von Wiren N. 2020. Signaling pathways underlying nitrogen-dependent changes in root system architecture: from model to crop species. *Journal of Experimental Botany* **71**: 4393-404.

Khan MA, Gemenet DC, Villordon A. 2016. Root system architecture and abiotic stress tolerance: current knowledge in root and tuber crops. *Frontiers in Plant Science* **7**: 1584.

Kieber JJ, Schaller GE. 2018. Cytokinin signaling in plant development. *Development* **145**.

Ko D, Kang J, Kiba T, Park J, Kojima M, Do J, Kim KY, Kwon M, Endler A, Song WY, et al. 2014. *Arabidopsis* ABCG14 is essential for the root-to-shoot translocation of cytokinin. *Proceedings of the National Academy of Sciences, USA* **111**: 7150-5.

Krishnan SR, Priya AM, Ramesh M. 2013. Rapid regeneration and ploidy stability of 'cv IR36' indica rice (*Oryza Sativa*. L) confers efficient protocol for in vitro callus organogenesis and Agrobacterium tumefaciens mediated transformation. *Botanical Studies* **54**: 47.

Kurakawa T, Ueda N, Maekawa M, Kobayashi K, Kojima M, Nagato Y, Sakakibara H, Kyozuka J. 2007. Direct control of shoot meristem activity by a cytokinin-activating enzyme. *Nature* **445**: 652-5.

Kurepa J, Smalle JA. 2022. Auxin/Cytokinin antagonistic control of the shoot/root growth ratio and its relevance for adaptation to drought and nutrient deficiency stresses. *International Journal of Molecular Sciences* **23**.

Kurihara D, Mizuta Y, Sato Y, Higashiyama T. 2015. ClearSee: a rapid optical clearing reagent for

whole-plant fluorescence imaging. *Development* **142**: 4168-79.

Laplaze L, Benkova E, Casimiro I, Maes L, Vanneste S, Swarup R, Weijers D, Calvo V, Parizot B, Herrera-Rodriguez MB, et al. 2007. Cytokinins act directly on lateral root founder cells to inhibit root initiation. *The Plant Cell* **19**: 3889-900.

Li B, Li G, Kronzucker HJ, Baluska F, Shi W. 2014. Ammonium stress in *Arabidopsis*: signaling, genetic loci, and physiological targets. *Trends in Plant Science* **19**: 107-14.

Li B, Li Q, Su Y, Chen H, Xiong L, Mi G, Kronzucker HJ, Shi W. 2011. Shoot-supplied ammonium targets the root auxin influx carrier AUX1 and inhibits lateral root emergence in *Arabidopsis*. *Plant Cell and Environment* **34**: 933-46.

Li G, Zhang L, Wu J, Yue X, Wang M, Sun L, Di D, Kronzucker HJ, Shi W. 2022. OsEIL1 protects rice growth under NH_4^+ nutrition by regulating OsVTC1-3-dependent N-glycosylation and root NH_4^+ efflux. *Plant Cell & Environment* **45**: 1537-53.

Li Q, Li BH, Kronzucker HJ, Shi WM. 2010. Root growth inhibition by NH_4^+ in *Arabidopsis* is mediated by the root tip and is linked to NH_4^+ efflux and GMPase activity. *Plant Cell and Environment* **33**: 1529-42.

Liu B, Wu J, Yang S, Schiefelbein J, Gan Y. 2020. Nitrate regulation of lateral root and root hair development in plants. *Journal of Experimental Botany* **71**: 4405-14.

Liu XX, Zhang HH, Zhu QY, Ye JY, Zhu YX, Jing XT, Du WX, Zhou M, Lin XY, Zheng SJ, et al. 2022. Phloem iron remodels root development in response to ammonium as the major nitrogen source. *Nature Communications* **13**: 561.

Liu Y, Maniero RA, Giehl RFH, Melzer M, Steensma P, Krouk G, Fitzpatrick TB, von Wirén N. 2022. PDX1.1-dependent biosynthesis of vitamin B(6) protects roots from ammonium-induced oxidative stress. *Molecular Plant* **15**: 820-39.

Luo L, Zhu M, Jia L, Xie Y, Wang Z, Xuan W. 2022. Ammonium transporters cooperatively regulate rice crown root formation responding to ammonium nitrogen. *Journal of Experimental Botany* **73**: 3671-85.

Ma X, Yan H, Yang J, Liu Y, Li Z, Sheng M, Cao Y, Yu X, Yi X, Xu W, et al. 2022. PlantGSAD: a comprehensive gene set annotation database for plant species. *Nucleic Acids Research* **50**: D1456-D67.

Mao C, He J, Liu L, Deng Q, Yao X, Liu C, Qiao Y, Li P, Ming F. 2020. OsNAC2 integrates auxin and cytokinin pathways to modulate rice root development. *Plant Biotechnology Journal* **18**: 429-42.

Maqbool S, Hassan MA, Xia X, York LM, Rasheed A, He Z. 2022. Root system architecture in cereals: progress, challenges and perspective. *The Plant Journal* **110**: 23-42.

Meng F, Zhao Q, Zhao X, Yang C, Liu R, Pang J, Zhao W, Wang Q, Liu M, Zhang Z, et al. 2022. A rice protein modulates endoplasmic reticulum homeostasis and coordinates with a transcription factor to initiate blast disease resistance. *Cell Reports* **39**: 110941.

Meier M, Liu Y, Lay-Pruitt KS, Takahashi H, von Wirén N. 2020. Auxin-mediated root branching is determined by the form of available nitrogen. *Nature Plants* **6**: 1136-45.

Miao J, Guo D, Zhang J, Huang Q, Qin G, Zhang X, Wan J, Gu H, Qu LJ. 2013. Targeted mutagenesis in rice using CRISPR-Cas system. *Cell Research* **23**: 1233-6.

Motte H, Vanneste S, Beeckman T. 2019. Molecular and environmental regulation of root development.

Annual Review of Plant Biology **70**: 465-88.

O'Brien JA, Vega A, Bouguyon E, Krouk G, Gojon A, Coruzzi G, Gutierrez RA. 2016. Nitrate transport, sensing, and responses in plants. *Molecular Plant* **9**: 837-56.

Patterson K, Cakmak T, Cooper A, Lager I, Rasmusson AG, Escobar MA. 2010. Distinct signalling pathways and transcriptome response signatures differentiate ammonium- and nitrate-supplied plants. *Plant Cell and Environment* **33**: 1486-501.

Poitout A, Crabos A, Petrik I, Novak O, Krouk G, Lacombe B, Ruffel S. 2018. Responses to systemic nitrogen signaling in a *Arabidopsis* roots involve trans-zeatin in shoots. *Plant Cell* **30**: 1243-57.

Qin C, Qian W, Wang W, Wu Y, Yu C, Jiang X, Wang D, Wu P. 2008. GDP-mannose pyrophosphorylase is a genetic determinant of ammonium sensitivity in *Arabidopsis thaliana*. *Proceedings of the National Academy of Sciences, USA* **105**: 18308-13.

Rogers ED, Benfey PN. 2015. Regulation of plant root system architecture: implications for crop advancement. *Current Opinion in Biotechnology* **32**: 93-8.

Rong C, Liu Y, Chang Z, Liu Z, Ding Y, Ding C, Zhang J. 2022. Cytokinin oxidase/dehydrogenase family genes exhibit functional divergence and overlap in rice growth and development, especially in control of tillering. *Journal of Experimental Botany* **73**: 3552-68.

Ruffel S, Krouk G, Ristova D, Shasha D, Birnbaum KD, Coruzzi GM. 2011. Nitrogen economics of root foraging: transitive closure of the nitrate-cytokinin relay and distinct systemic signaling for N supply vs. demand. *Proceedings of the National Academy of Sciences*, *USA* **108**: 18524-9.

Ruzicka K, Simaskova M, Duclercq J, Petrasek J, Zazimalova E, Simon S, Friml J, Van Montagu MC, Benkova E. 2009. Cytokinin regulates root meristem activity via modulation of the polar auxin transport. *Proceedings of the National Academy of Sciences*, *USA* **106**: 4284-9.

Schmülling T, Werner T, Riefler M, Krupková E, Bartrina y Manns I. 2003. Structure and function of cytokinin oxidase/dehydrogenase genes of maize, rice, *Arabidopsis* and other species. *Journal of Plant Research* **116**: 241-52.

Su YH, Liu YB, Zhang XS. 2011. Auxin-cytokinin interaction regulates meristem development. *Molecular Plant* **4**: 616-25.

Sun L, Di DW, Li G, Kronzucker HJ, Wu X, Shi W. 2020. Endogenous ABA alleviates rice ammonium toxicity by reducing ROS and free ammonium via regulation of the SAPK9-bZIP20 pathway. *Journal of Experimental Botany* **71**: 4562-77.

Taylor I, Lehner K, McCaskey E, Nirmal N, Ozkan-Aydin Y, Murray-Cooper M, Jain R, Hawkes EW, Ronald PC, Goldman DI, et al. 2021. Mechanism and function of root circumnutation. *Proceedings of the National Academy of Sciences, USA* **118**.

Tsai Y-C, Weir NR, Hill K, Zhang W, Kim HJ, Shiu S-H, Schaller GE, Kieber JJ. 2012. Characterization of genes involved in cytokinin signaling and metabolism from rice. *Plant Physiology* **158**: 1666-84.

Wu XX, Yuan P, Chen H, Kumar V, Kang SM, Jia B, Xuan YH. 2022. Ammonium transporter 1 increases rice resistance to sheath blight by promoting nitrogen assimilation and ethylene signalling. *Plant Biotechnology Journal* **20**: 1085-97.

Xie Y, Lv Y, Jia L, Zheng L, Li Y, Zhu M, Tian M, Wang M, Qi W, Luo L, et al. 2023. Plastid-

localized amino acid metabolism coordinates rice ammonium tolerance and nitrogen use efficiency. *Nature Plants* **9**: 1514-29.

Xu G, Fan X, Miller AJ. 2012. Plant nitrogen assimilation and use efficiency. *Annual Review of Plant Biology* **63**: 153-82.

Xu W, Jia L, Shi W, Liang J, Zhou F, Li Q, Zhang J. 2013. Abscisic acid accumulation modulates auxin transport in the root tip to enhance proton secretion for maintaining root growth under moderate water stress. *New Phytologist* **197**: 139-50.

Xuan W, Beeckman T, Xu G. 2017. Plant nitrogen nutrition: sensing and signaling. *Current Opinion in Plant Biology* **39**: 57-65.

Xuan YH, Priatama RA, Huang J, Je BI, Liu JM, Park SJ, Piao HL, Son DY, Lee JJ, Park SH, et al. 2012. Indeterminate domain 10 regulates ammonium mediated gene expression in rice roots. *New Phytologist* **197**: 791-804.

Yang B, Minne M, Brunoni F, Plačková L, Petřík I, Sun Y, Nolf J, Smet W, Verstaen K, Wendrich JR, et al. 2021. Non-cell autonomous and spatiotemporal signalling from a tissue organizer orchestrates root vascular development. *Nature Plants* **7**: 1485-94.

Yang J, Yuan Z, Meng Q, Huang G, Perin C, Bureau C, Meunier AC, Ingouff M, Bennett MJ, Liang W, et al. 2017. Dynamic regulation of auxin response during rice development revealed by newly established hormone biosensor markers. *Frontiers in Plant Science* **8**: 256.

Yeh SY, Chen HW, Ng CY, Lin CY, Tseng TH, Li WH, Ku MS. 2015. Down-regulation of cytokinin oxidase 2 expression increases tiller number and improves rice yield. *Rice* **8**: 36.

Zhang K, Novak O, Wei Z, Gou M, Zhang X, Yu Y, Yang H, Cai Y, Strnad M, Liu CJ. 2014. *Arabidopsis* ABCG14 protein controls the acropetal translocation of root-synthesized cytokinins. *Nature Communications* **5**: 3274.

Zhao H, Duan KX, Ma B, Yin CC, Hu Y, Tao JJ, Huang YH, Cao WQ, Chen H, Yang C, et al. 2020. Histidine kinase MHZ1/OsHK1 interacts with ethylene receptors to regulate root growth in rice. *Nature Communications* **11**: 518.

Zurcher E, Tavor-Deslex D, Lituiev D, Enkerli K, Tarr PT, Muller B. 2013. A robust and sensitive synthetic sensor to monitor the transcriptional output of the cytokinin signaling network in planta. *Plant Physiology* **161**: 1066-75.

Supporting Information

Fig. S1 Transcriptome data analysis of rice NIP roots after high and low NH_4^+ treatments by volcano plot and KEGG classification.

Fig. S2 Expression pattern of *CKX3* in rice roots.

Fig. S3 Subcellar localization of CKX3 in rice protoplast.

Fig. S4 Detailed information of loss-of-function mutant alleles of *CKX3* and *CKX8* generated by CRISPR/Cas9 gene editing.

Fig. S5 The effects of NH_4^+ on the root development of NIP and *CKX3* overexpression lines.

Fig. S6 Phylogenetic trees of CKX family in rice and Arabidopsis.

Fig. S7 The effects of high ammonium on the expression of cytokinin biosynthesis genes in rice root.

Fig. S8 Detailed information of loss-of-function double mutant alleles of *RR25* and *RR26* generated by CRISPR/Cas9 gene editing.

Fig. S9 Quantifications of the contents of IAA, IBA and cytokinin derivatives iP, tZ, cZ, cZR and iPR in the roots of germinated NIP and *rr25-1rr26-1* seedlings grown under LN and HN conditions for 7 days.

Fig. S10 The effects of 6-BA on the root phenotypes of NIP and *rr25-1rr26-1* seedlings under LN and HN conditions.

Fig. S11 Heatmap showing the expression of NH_4^+-responsive transcription factors in the roots of NIP seedlings under LN and HN condition after 6 h and 24 h treatments.

Fig. S12 Predicted binding sites of indicated transcription factors in the promoter region of *CKX3*.

Table S1 Primers used for constructing vectors.

Table S2 Differentially expressed genes in the roots of NIP seedlings under low NH_4^+ (LN) and high NH_4^+ (HN) treatments for 6 h and 24 h.

Table S3 Primers used for qRT-PCR.

Figure Legends

Fig. 1 Transcriptome analysis of rice NIP roots after high and low NH_4^+ treatments. (a) Diagram of sampling process for transcriptome analysis. 4-day-old NIP seedling were treated with 0.125 mM or 1.25 mM $(NH_4)_2SO_4$ for 6 h and 24 h, and then the root tips were collected for RNA-seq. (b) Venn diagram of differently expressed genes in roots after 6 h and 24 h NH_4^+ treatments. (c) Top enriched GO pathways of the DEGs identified in (b). Y-axis represents biological functions; X-axis represents the number of DEGs; The color bar at the right indicates the range of -log10 (*p*-value). (d) Heatmap showing the expressions of CKX family genes under LN and HN condition after 6 h and 24 h treatments. The color bar at the bottom indicates Z-score. LN, 0.125 mM $(NH_4)_2SO_4$; HN, 1.25 mM $(NH_4)_2SO_4$.

Fig. 2 The effects of NH_4^+ on the expression pattern of *CKX3* in root. (a) Relative expression levels of *CKX* family genes in the roots of 4-day-old NIP seedlings grown under LN and HN conditions for another 24 h (n = 6 biological replicates). (b) Time course analysis of *CKX3* expression in the root of 4-day-old NIP seedlings grown under LN and HN conditions over 48 h (n = 3 biological replicates). (c) Detection of GUS activity in roots of 4-day-old *pCKX3:GUS* transgenic lines grown under LN and HN conditions for 24 h. Scale bar, 3 mm. (d) Detection of GUS activity in lateral root primordia of *pCKX3:GUS* transgenic lines showing in (c). Scale bar, 50 μm. LN, 0.125 mM $(NH_4)_2SO_4$; HN, 1.25 mM $(NH_4)_2SO_4$. Data are means ± SD. Asterisks indicate significant difference by Student's *t* test (*, $P < 0.05$; **, $P < 0.01$; ***, $P < 0.001$).

Fig. 3 The effects of NH_4^+ on the root development of *CKX3* mutants. (a) Images showing the root phenotypes of germinated NIP, *ckx3-1*, *ckx3-2* and *ckx3-3* seeds grown under LN and HN conditions for 7 days. The lower panels are high magnification of the dot-boxed areas in upper panels. Scale bar, 1 cm. (b and c) Quantification of relative lateral root density (b) and relative seminal root length (c) by normalizing to WT under LN conditions in the indicated genotypes showing in (a). LN, 0.125 mM $(NH_4)_2SO_4$; HN, 1.25 mM $(NH_4)_2SO_4$. Data are means ± SD (n = 15 individual seedlings). Asterisks indicate significant difference by Student's t test (*, $P < 0.05$; **, $P < 0.01$; ***, $P < 0.001$; ns, not significant); percentage values above the column indicate the increased/decreased percentages by HN treatment in relation to LN treatment.

Fig. 4 The effects of NH_4^+ on the root meristem activity in *CKX3* mutants. (a) Confocal images of root meristems of 3-day-old NIP, *ckx3-1*, *ckx3-2* and *ckx3-3* seedlings grown under LN and HN conditions for another 4 days. Yellow and white arrowheads indicate the location of stem cells and the cortex cells at start of elongation zone, respectively. Scale bar, 100 μm. (b) Quantifications of meristem cortical cell number (b) and meristem length (c) in the indicated genotypes showing in (a). LN, 0.125 mM $(NH_4)_2SO_4$; HN, 1.25 mM $(NH_4)_2SO_4$. Data are means ± SD (n = 10 individual seedlings). Asterisks indicate significant difference by Student's *t* test (*, $P < 0.05$; **, $P < 0.01$; ***, $P < 0.001$); percentage values above the column indicate the increased/decreased percentages by HN treatment in relation to LN treatment.

Fig. 5 The effects of NH_4^+ on the root development of *CKX3* and *CKX8* mutants. (a) Images showing the root phenotypes of germinated NIP, *ckx3-1*, *ckx8-1* and *ckx3-1ckx8-1* seeds grown under LN and HN conditions for 7 days. The lower panels are high magnification of the dot-boxed areas in upper panels. Scale bar, 5 mm. (b and c) Quantifications of relative lateral root density and relative seminal root length

by normalizing to WT under LN conditions of indicated rice seedlings showing in (a). LN, 0.125 mM $(NH_4)_2SO_4$; HN, 1.25 mM $(NH_4)_2SO_4$. Data are means ± SD (n = 10 individual seedlings). Asterisks indicate significant difference by Student's *t* test (*, $P < 0.05$; **, $P < 0.01$; ***, $P < 0.001$; ns, not significant); percentage values above the column indicate the increased/decreased percentages by HN treatment in relation to LN treatment.

Fig. 6 The effects of NH_4^+ on the contents of cytokinin derivates in the root of *ckx3-1*, *ckx8-1* and *ckx3-1ckx8-1*. (a) Quantifications of the contents of cytokinin derivatives iP, tZ, cZ, cZR and iPR in the roots of germinated NIP, *ckx3-1*, *ckx8-1* and *ckx3-1ckx8-1* seeds grown under LN and HN conditions for 7 days. (b and c) Detection of *TCSn:GUS* activity in the lateral roots (upper panels) and root tips (low panels) of 4-day-old NIP and *ckx3-1* seedlings grown under LN and HN conditions for another 1 day. Scale bar, 200 μm. Red triangles indicates lateral roots. LN, 0.125 mM $(NH_4)_2SO_4$; HN, 1.25 mM $(NH_4)_2SO_4$. Data are means ± SD (n = 3 biological replicates). Different lowercase letters above columns indicate significant differences ($P < 0.05$, ANOVA followed by Tukey test).

Fig. 7 The effects of 6-BA and iP on the root phenotypes of *CKX3* mutant and the expressions of *CKX3* and *CKX8* under low and high NH_4^+ conditions. (a) Images showing the root phenotypes of germinated NIP and *ckx3-1* seeds grown under LN and HN conditions, in the presence or absence of 10 nM 6-BA and 100 nM iP for 7 days. The lower panels are high magnification of the dot-boxed areas in upper panels. Scale bar, 1 cm. (b) Quantifications of relative lateral root density and relative seminal root length by normalizing to WT under LN conditions in the indicated seedlings showing in (a) (n = 10 individual seedlings). Percentage values above the column indicate the increased/decreased percentages by HN treatment in relation to LN treatment. (c) Quantification of *CKX3* and *CKX8* expression levels in the root of 4-day-old NIP seedling that were further transferred to the medium containing 10 nM 6-BA or 100 nM iP for indicated times (n = 3 biological replicates). LN, 0.125 mM $(NH_4)_2SO_4$; HN, 1.25 mM $(NH_4)_2SO_4$. Data are means ± SD. Asterisks indicate significant difference by Student's *t* test (*, $P < 0.05$; **, $P < 0.01$; ***, $P < 0.001$; nd, no data; ns, not significant).

Fig. 8 The regulation of B-type Cytokinin response regulators RR25 and RR26 in the expression of *CKX3* and rice root responses to external NH_4^+. (a) Heatmap showing the expressions of B-type RR family genes under HN and LN condition after 6 h and 24 h treatments. The color bar at the bottom indicates Z-score. (b) Sequence and location of cytokinin response elements in the promoter of *CKX3*. The purple squares represent five cytokinin response elements in the promoter of *CKX3*. (c) Yeast-one-hybrid assay showing the binding of *CKX3* promoter by RR25 and RR26 in yeast. The promoter of *CKX3* was integrated into yeast genomic DNA as bait vectors, then RR25, RR26 or empty vector was independently transformed into yeast containing the bait vector. (d) Transient transactivation assay of *pCKX3:LUC* with RR25 and RR26 in tobacco leaf. Plasmids containing the effector and reporter vectors were co-transferred into Agrobacterium-mediated tobacco leaves. Circular dashed lines indicate sites of Agrobacterium inoculation. The pseudo-color bar indicates the range of luminescence intensity. Scale bar, 5 mm. (e) Transient transactivation assay of *pCKX3:LUC* with RR25 and RR26 in rice protoplasts. Plasmids containing the effector and reporter vectors were transfected into rice protoplasts. Effector and reporter vector were Renilla luciferase (REN) and LUC activities were detected by the Dual-luciferase ® reporter assay system (n = 3 biological replicates). (f) Quantification of expression of *CKX3* expression

levels in the roots of NIP and *rr25-1rr26-1* seedling. 4-day-old NIP and *rr25-1rr26-1* seedlings grown under LN and HN conditions for another 24 h (n = 3 biological replicates). Different lowercase letters above columns indicate significant differences ($P < 0.05$, ANOVA followed by Tukey test). (g) Images showing the root phenotypes of germinated NIP, *rr25-1rr26-1*, and *rr25-2rr26-2* seeds grown under LN and HN condition for 7 days. Scale bar, 5 mm. (h) Quantifications of relative lateral root density and relative seminal root length by normalizing to WT under LN conditions in the indicated seedlings showing in (g). LN, 0.125 mM $(NH_4)_2SO_4$; HN, 1.25 mM $(NH_4)_2SO_4$. Data are means ± SD (n = 10 individual seedlings). Asterisks indicate significant difference by Student's t test (*, $P < 0.05$; **, $P < 0.01$; ***, $P < 0.001$); percentage values above the column indicate the increased/decreased percentages by HN treatment in relation to LN treatment.

Fig. 9 The effects of NH_4^+ and exogenous cytokinins on the *DR5* expression in the root tip of *CKX3* mutant. (a) Confocal images of *DR5rev:3xVENUS-N7* signal in the root tips of 4-day-old NIP and *ckx3-1* seedlings grown under LN and HN conditions, in the presence and absence of 10 nM 6-BA or iP for another 1 day. Yellow and red triangles indicate the root epidermis and the stele, respectively. Scale bar, 100 μm. (b) Quantification of *DR5rev:3xVENUS-N7* signaling in root epidermis and stele of the indicated seedlings showing in (a). LN, 0.125 mM $(NH_4)_2SO_4$; HN, 1.25 mM $(NH_4)_2SO_4$. Data are means ± SD (n = 10 individual seedlings). Different lowercase letters above columns indicate significant differences ($P < 0.05$, ANOVA followed by Tukey test).

Fig. 10 The effects of NH_4^+ and exogenous cytokinins on the *DR5* expression in the lateral root primordia of *CKX3* mutant. (a) Confocal images of *DR5rev:3xVENUS-N7* signal in the lateral root primordia of 4-day-old NIP and *ckx3-1* seedlings grown under LN and HN conditions, in the presence and absence of 10 nM 6-BA or iP for another 1 day. Red triangles indicate the position of lateral root primordia. Scale bar, 100 μm. (b) Quantification of *DR5rev:3xVENUS-N7* signaling in the lateral root primordia of indicated seedlings showing in (a) (n = 10 biological replicates). (c) Quantification of the content of IAA and IBA in the roots of germinated NIP and *ckx3-1* seeds grown under LN and HN conditions for another 7 days (n = 3 biological replicates). LN, 0.125 mM $(NH_4)_2SO_4$; HN, 1.25 mM $(NH_4)_2SO_4$. Data are means ± SD. Different lowercase letters above columns indicate significant differences ($P < 0.05$, ANOVA followed by Tukey test).

Fig. 11 A working model for CKX3-mediated root growth responses to external high NH_4^+ supply. Cytokinin (CK) accumulation causes inhibition on auxin signaling/homeostasis and root development; CKXs act on the degradation of endogenous CKs, and play critical roles in regulating endogenous CK levels. In this model, the expression of CK biosynthesis pathway genes are induced by high NH_4^+, accompanied with increased level of endogenous CK derivates, which led to shorter seminal root elongation and higher lateral root density. The *CKX3* and its homologue *CKX8*, are transcriptional activated by B-type Response Regulator (RR) genes *RR25* and *RR26* under high NH_4^+ to reduce endogenous CK levels, in turn attenuating the effects of NH_4^+ on root growth. While the knock-out mutants of *CKX3* and *CKX8* has reduced seminal root elongation and lateral root formation under either high or low NH_4^+ condition, due to the accumulation of CKs *in vivo*, thus exhibiting reduced root sensitivity to high NH_4^+. Furthermore, CKX3 can also be targeted and regulated by other NH_4^+-responsive transcription factors (TFs), and other CKX family members may also play roles in regulating

root responses to external NH_4^+. The balck pointed and blunt-ended arrows represent positive and negative regulations, respectviely; the black dotted arrow indicates unknown interaction based on transcriptome data; the solid red arrow indicates increase of CK level.

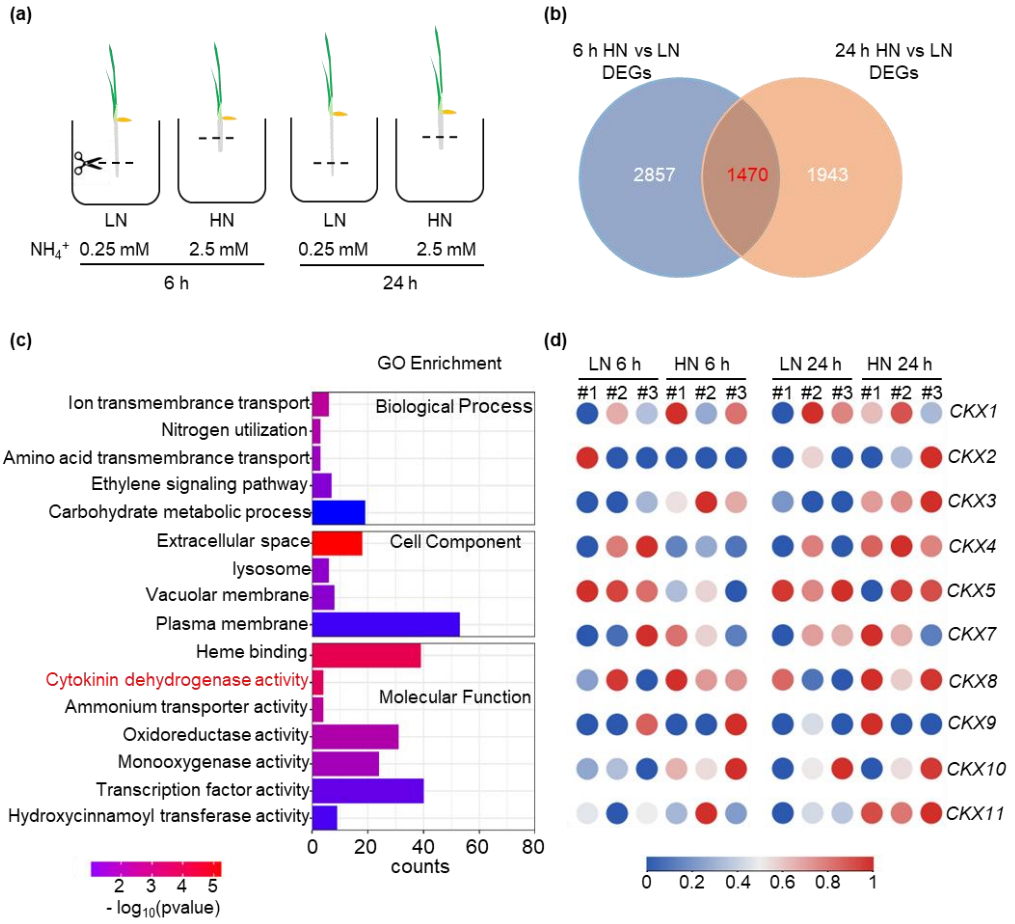

Fig. 1 Transcriptome analysis of rice NIP roots after high and low NH_4^+ treatments. (a) Diagram of sampling process for transcriptome analysis. 4-day-old NIP seedling were treated with 0.125 mM or 1.25 mM $(NH_4)_2SO_4$ for 6 h and 24 h, and then the root tips were collected for RNA-seq. (b) Venn diagram of differently expressed genes in roots after 6 h and 24 h NH_4^+ treatments. (c) Top enriched GO pathways of the DEGs identified in (b). Y-axis represents biological functions; X-axis represents the number of DEGs; The color bar at the right indicates the range of -log10 (pvalue). (d) Heatmap showing the expressions of CKX family genes under HN and LN condition after 6 h and 24 h treatments. The color bar at the bottom indicates Z-score. HN, 1.25 mM $(NH_4)_2SO_4$; LN, 0.125 mM $(NH_4)_2SO_4$.

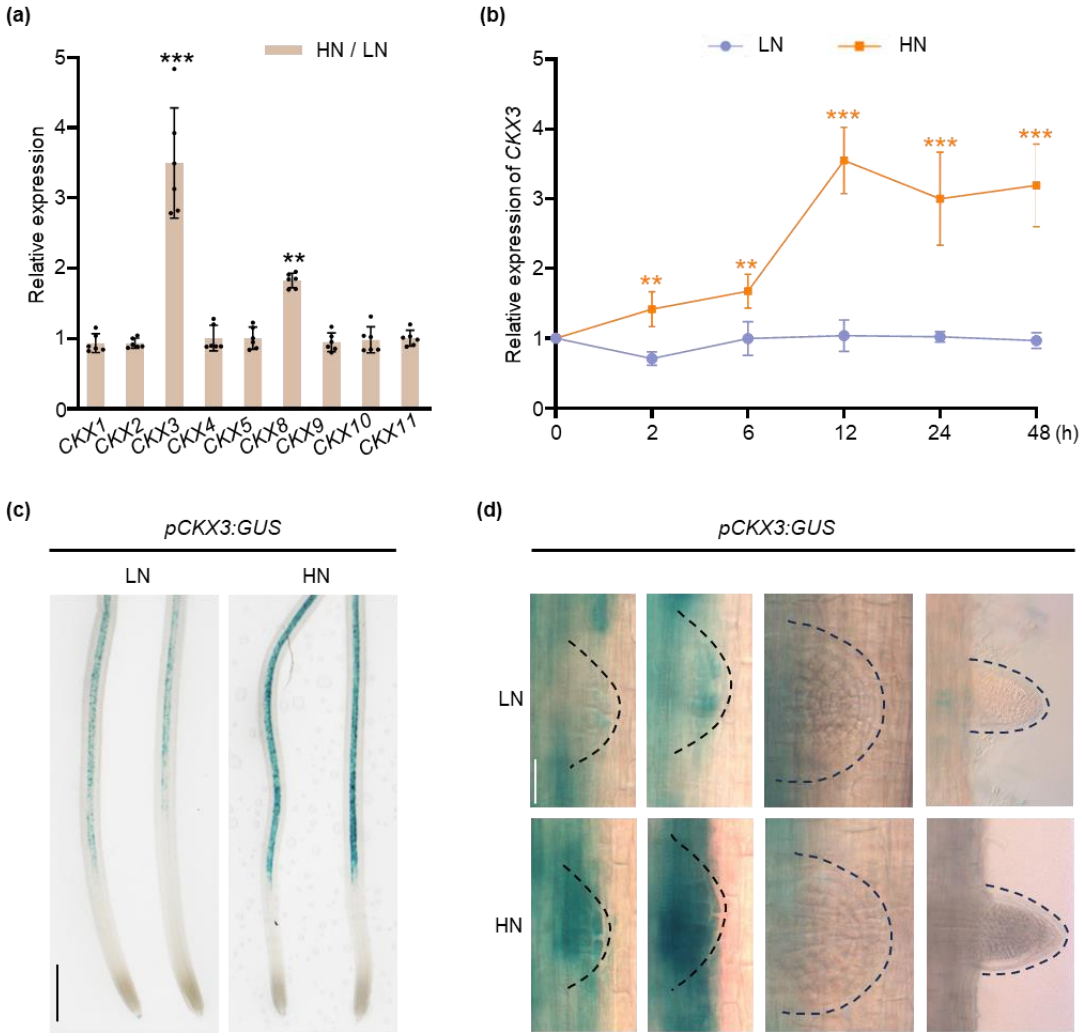

Fig. 2 The effects of NH_4^+ on the expression pattern of *CKX3* in root. (a) Relative expression levels of *CKX* family genes in the roots of 4-day-old NIP seedlings grown under LN and HN conditions for another 24 h (n = 6 biological replicates). (b) Time course analysis of *CKX3* expression in the root of 4-day-old NIP seedlings grown under LN and HN conditions over 48 h (n = 3 biological replicates). (c) Detection of GUS activity in roots of 4-day-old *pCKX3:GUS* transgenic lines grown under LN and HN conditions for 24 h. Scale bar, 3 mm. (d) Detection of GUS activity in lateral root primordia of *pCKX3:GUS* transgenic lines showing in (c). Scale bar, 50 μm. LN, 0.125 mM $(NH_4)_2SO_4$; HN, 1.25 mM $(NH_4)_2SO_4$. Data are means ± SD. Asterisks indicate significant difference by Student's *t* test (*, $P < 0.05$; **, $P < 0.01$; ***, $P < 0.001$).

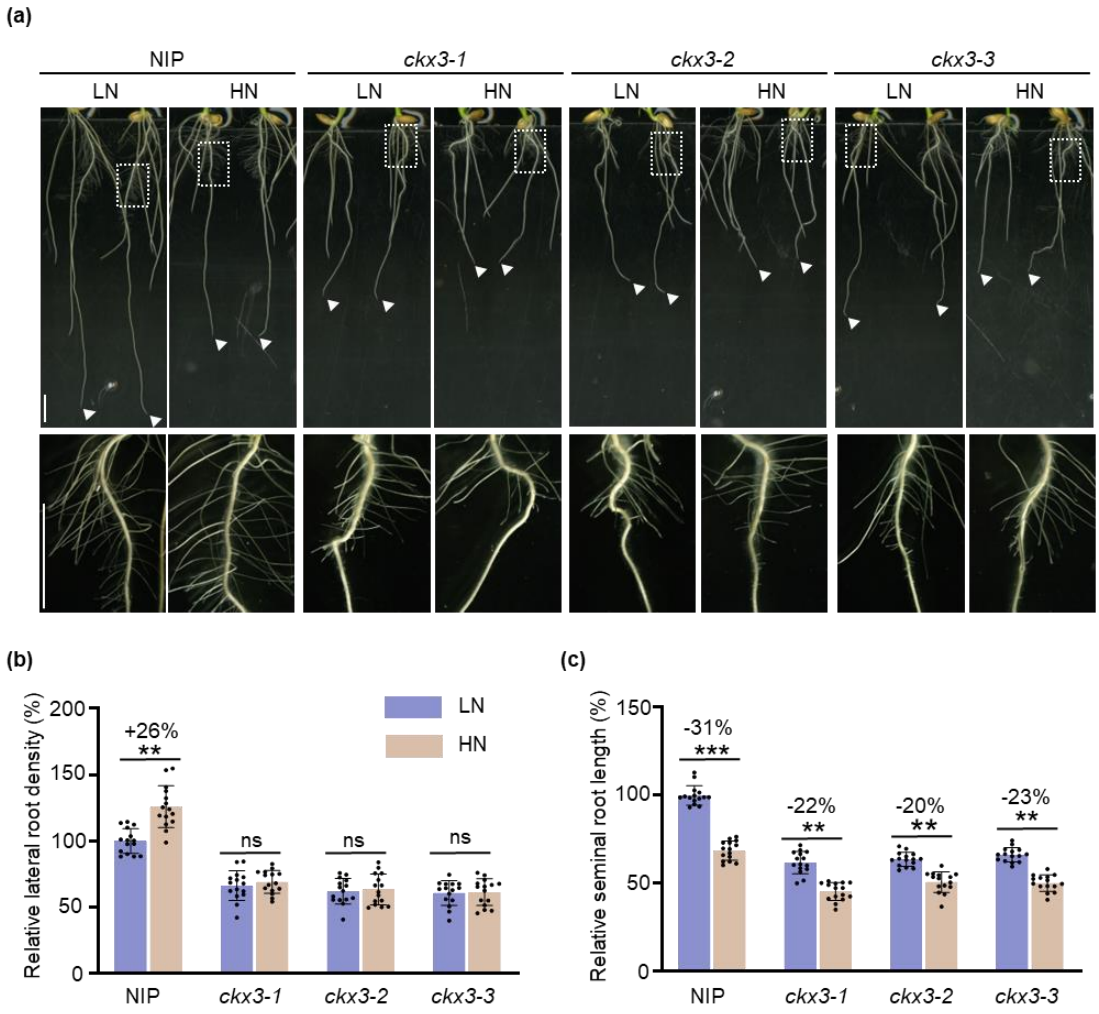

Fig. 3 The effects of NH_4^+ on the root development of *CKX3* mutants. (a) Images showing the root phenotypes of germinated NIP, *ckx3-1*, *ckx3-2* and *ckx3-3* seeds grown under LN and HN conditions for 7 days. The lower panels are high magnification of the dot-boxed areas in upper panels. Scale bar, 1 cm. (b and c) Quantification of relative lateral root density (b) and relative seminal root length (c) by normalizing to WT under LN conditions in the indicated genotypes showing in (a). LN, 0.125 mM $(NH_4)_2SO_4$; HN, 1.25 mM $(NH_4)_2SO_4$. Data are means ± SD (n = 15 individual seedlings). Asterisks indicate significant difference by Student's t test (*, $P < 0.05$; **, $P < 0.01$; ***, $P < 0.001$; ns, not significant); percentage values above the column indicate the increased/decreased percentages by HN treatment in relation to LN treatment.

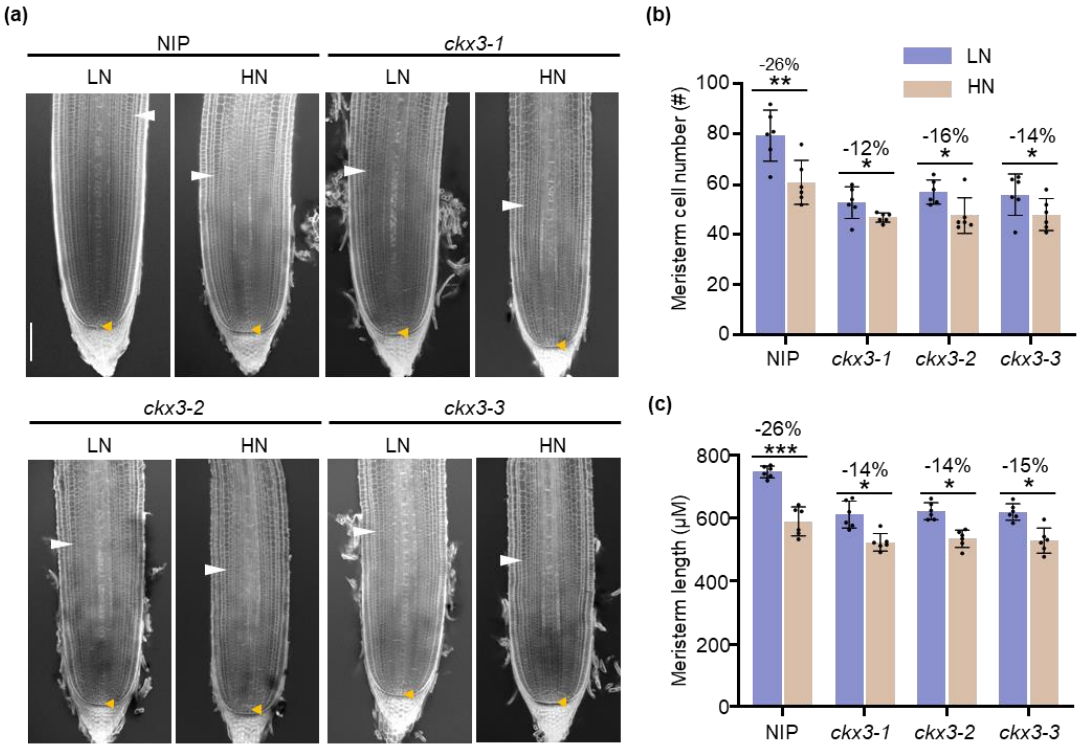

Fig. 4 The effects of NH_4^+ on the root meristem activity in *CKX3* mutants. (a) Confocal images of root meristems of 3-day-old NIP, *ckx3-1*, *ckx3-2* and *ckx3-3* seedlings grown under LN and HN conditions for another 4 days. Yellow and white arrowheads indicate the location of stem cells and the cortex cells at start of elongation zone, respectively. Scale bar, 100 μm. (b) Quantifications of meristem cortical cell number (b) and meristem length (c) in the indicated genotypes showing in (a). LN, 0.125 mM $(NH_4)_2SO_4$; HN, 1.25 mM $(NH_4)_2SO_4$. Data are means ± SD (n = 10 individual seedlings). Asterisks indicate significant difference by Student's *t* test (*, $P < 0.05$; **, $P < 0.01$; ***, $P < 0.001$); percentage values above the column indicate the increased/decreased percentages by HN treatment in relation to LN treatment.

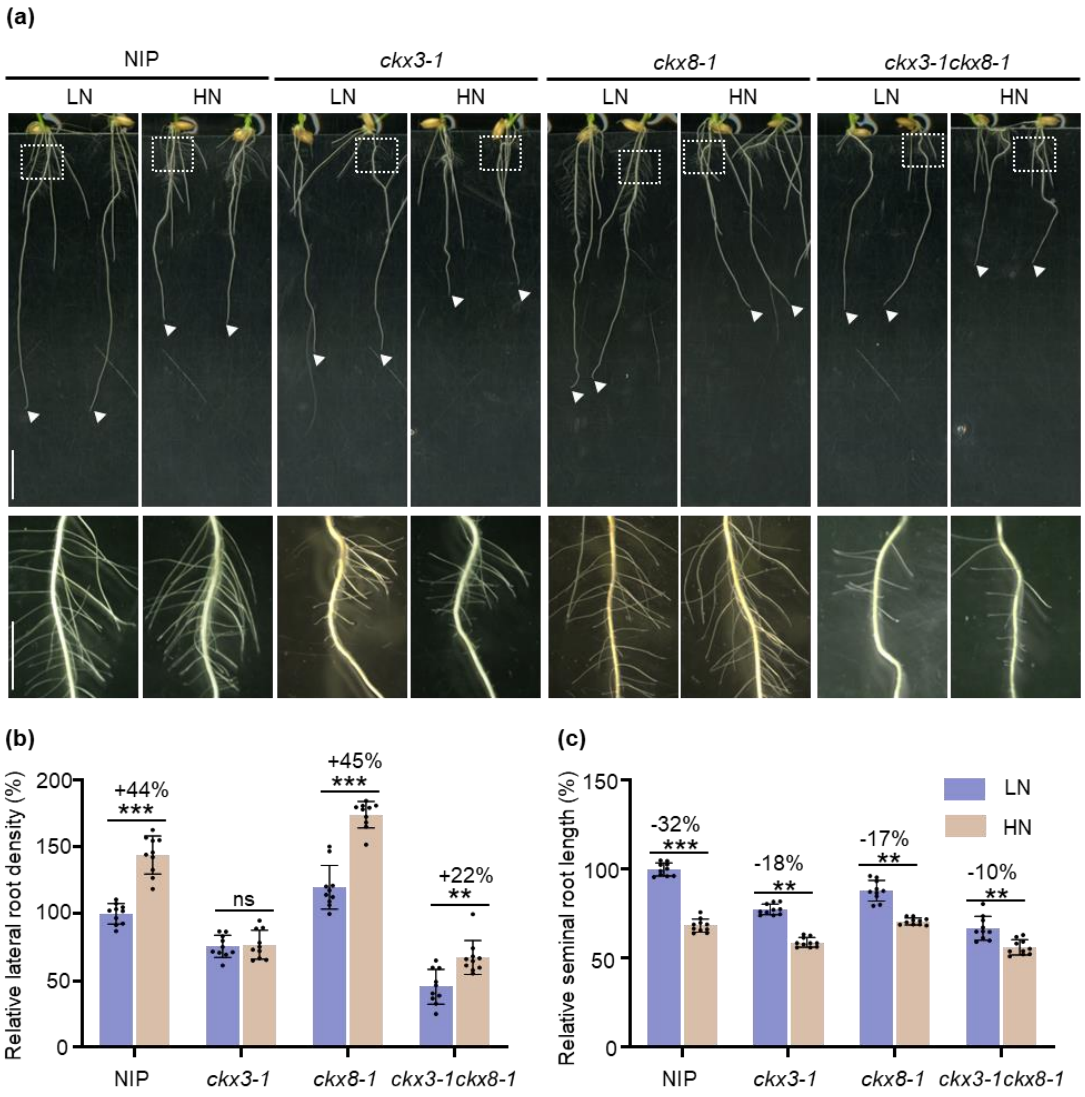

Fig. 5 The effects of NH_4^+ on the root development of *CKX3* and *CKX8* mutants. (a) Images showing the root phenotypes of germinated NIP, *ckx3-1*, *ckx8-1* and *ckx3-1ckx8-1* seeds grown under LN and HN conditions for 7 days. The lower panels are high magnification of the dot-boxed areas in upper panels. Scale bar, 5 mm. (b and c) Quantifications of relative lateral root density and relative seminal root length by normalizing to WT under LN conditions of indicated rice seedlings showing in (a). LN, 0.125 mM $(NH_4)_2SO_4$; HN, 1.25 mM $(NH_4)_2SO_4$. Data are means ± SD (n = 10 individual seedlings). Asterisks indicate significant difference by Student's *t* test (*, $P < 0.05$; **, $P < 0.01$; ***, $P < 0.001$; ns, not significant); percentage values above the column indicate the increased/decreased percentages by HN treatment in relation to LN treatment.

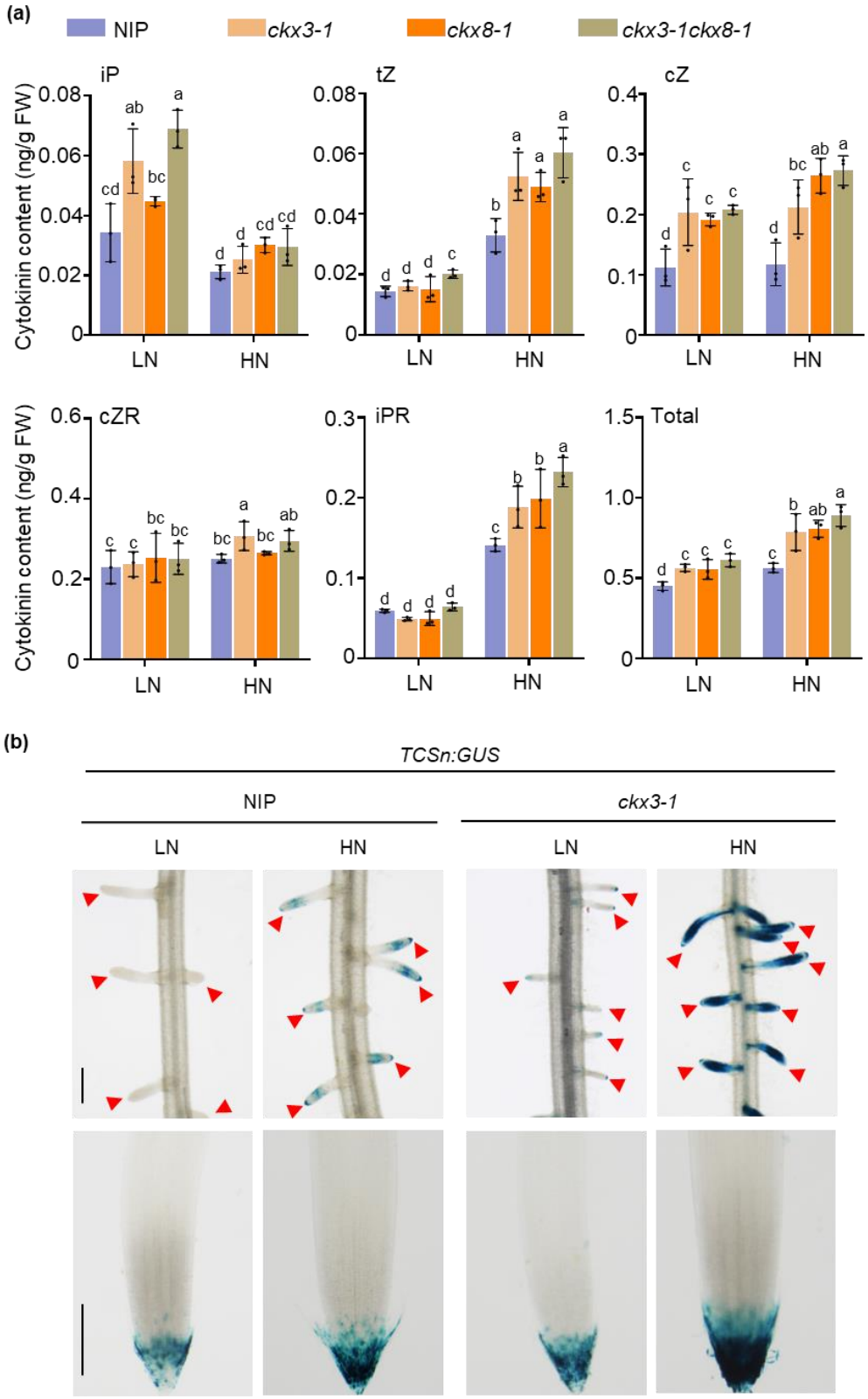

Fig. 6 The effects of NH_4^+ on the contents of cytokinin derivates in the root of *ckx3-1*, *ckx8-1* and *ckx3-1ckx8-1*. (a) Quantifications of the contents of cytokinin derivatives iP, tZ, cZ, cZR and iPR in the roots of germinated NIP, *ckx3-1*, *ckx8-1* and *ckx3-1ckx8-1* seeds grown under LN and HN conditions for 7 days. (b and c) Detection of *TCSn:GUS* activity in the lateral roots (upper panels) and root tips (low

panels) of 4-day-old NIP and *ckx3-1* seedlings grown under HN and LN conditions for another 1 day. Scale bar, 200 μm. Red triangles indicates lateral roots. Data are means ± SD (n = 3 biological replicates). Different lowercase letters above columns indicate significant differences ($P < 0.05$, ANOVA followed by Tukey test).

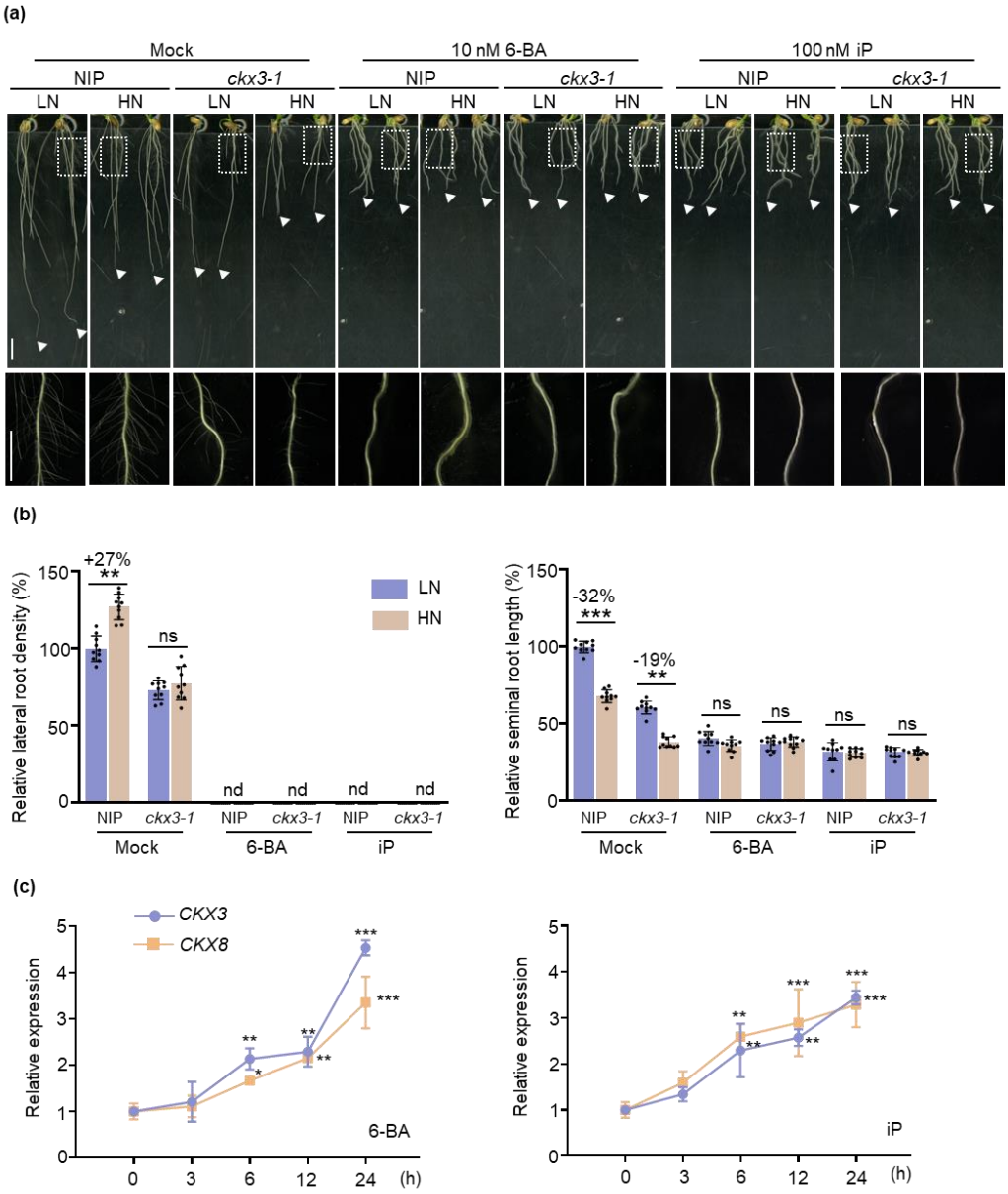

Fig. 7 The effects of 6-BA and iP on the root phenotypes of *CKX3* mutant and the expressions of *CKX3* and *CKX8* under high and low NH_4^+ conditions. (a) Images showing the root phenotypes of germinated NIP and *ckx3-1* seeds grown under LN and HN conditions, in the presence or absence of 10 nM 6-BA and 100 nM iP for 7 days. The lower panels are high magnification of the dot-boxed areas in upper panels. Scale bar, 1 cm. (b) Quantifications of relative lateral root density and relative seminal root length by normalizing to WT under LN conditions in the indicated seedlings showing in (a) (n = 10 individual seedlings). Percentage values above the column indicate the increased/decreased percentages by HN treatment in relation to LN treatment. (c) Quantification of *CKX3* and *CKX8* expression levels in the root of 4-day-old NIP seedling that were further transferred to the medium containing 10 nM 6-BA or 100 nM iP for indicated times (n = 3 biological replicates). LN, 0.125 mM $(NH_4)_2SO_4$; HN, 1.25 mM

$(NH_4)_2SO_4$. Data are means ± SD. Asterisks indicate significant difference by Student's *t* test (*, $P < 0.05$; **, $P < 0.01$; ***, $P < 0.001$; ns, not significant).

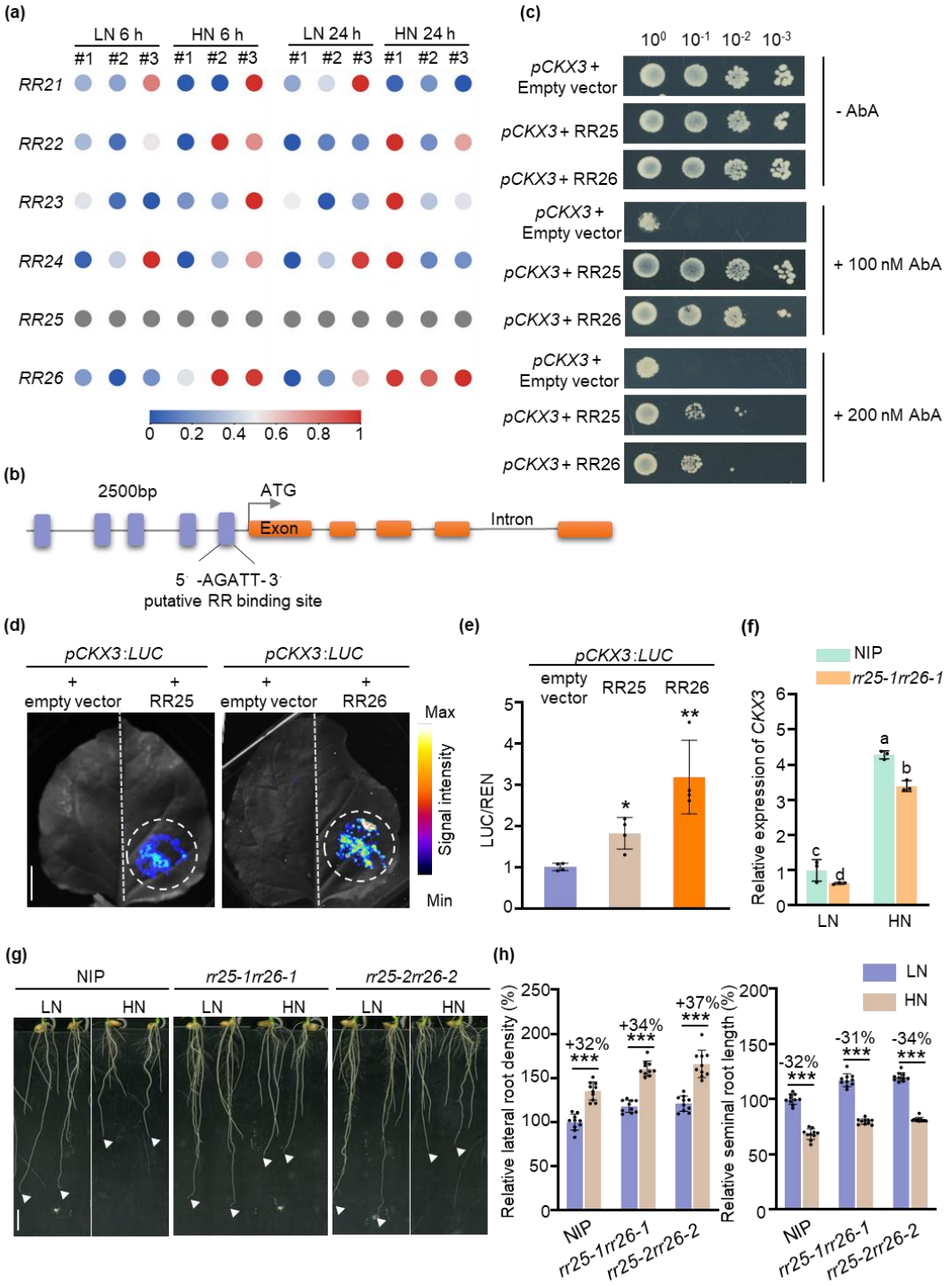

Fig. 8 The regulation of B-type Cytokinin response regulators RR25 and RR26 in the expression of *CKX3* and rice root responses to external NH_4^+. (a) Heatmap showing the expressions of B-type RR family genes under HN and LN condition after 6 h and 24 h treatments. The color bar at the bottom indicates Z-score. (b) Sequence and location of cytokinin response elements in the promoter of *CKX3*. The purple squares represent five cytokinin response elements in the promoter of *CKX3*. (c) Yeast-one-hybrid assay showing the binding of *CKX3* promoter by RR25 and RR26 in yeast. The

promoter of *CKX3* was integrated into yeast genomic DNA as bait vectors, then RR25, RR26 or empty vector was independently transformed into yeast containing the bait vector. (d) Transient transactivation assay of *pCKX3:LUC* with RR25 and RR26 in tobacco leaf. Plasmids containing the effector and reporter vectors were co-transferred into Agrobacterium-mediated tobacco leaves. Circular dashed lines indicate sites of Agrobacterium inoculation. The pseudo-color bar indicates the range of luminescence intensity. Scale bar, 5 mm. (e) Transient transactivation assay of *pCKX3:LUC* with RR25 and RR26 in rice protoplasts. Plasmids containing the effector and reporter vectors were transfected into rice protoplasts. Effector and reporter vector were Renilla luciferase (REN) and LUC activities were detected by the Dual-luciferase ® reporter assay system (n = 3 biological replicates). (f) Quantification of expression of *CKX3* expression levels in the roots of NIP and *rr25-1rr26-1* seedling. 4-day-old NIP and *rr25-1rr26-1* seedlings grown under LN and HN conditions for another 24 h (n = 3 biological replicates). (g) Images showing the root phenotypes of germinated NIP, *rr25-1rr26-1*, and *rr25-2rr26-2* seeds grown under LN and HN condition for 7 days. Scale bar, 5 mm. (h) Quantifications of relative lateral root density and relative seminal root length in the indicated seedlings showing in (g). LN, 0.125 mM $(NH_4)_2SO_4$; HN, 1.25 mM $(NH_4)_2SO_4$. Data are means ± SD (n = 10 individual seedlings). Asterisks indicate significant difference by Student's t test (*, $P < 0.05$; **, $P < 0.01$; ***, $P < 0.001$); percentage values above the column indicate the increased/decreased percentages by HN treatment in relation to LN treatment.

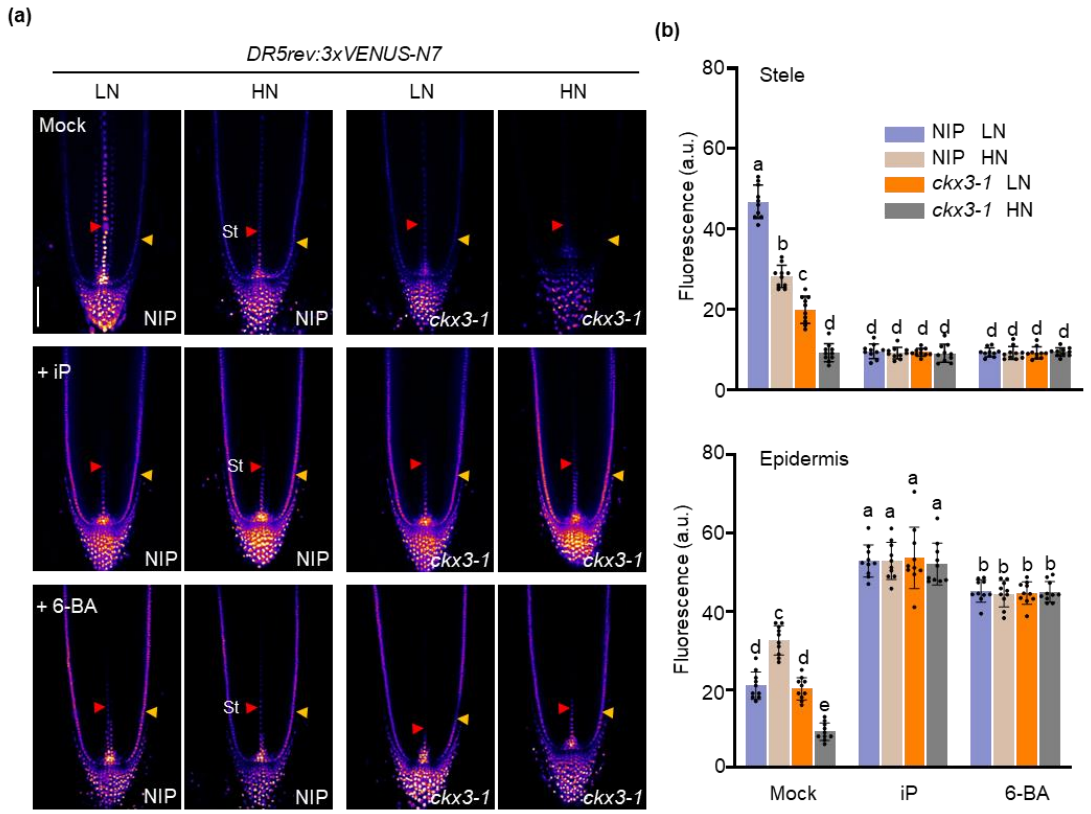

Fig. 9 The effects of NH_4^+ and exogenous cytokinins on the DR5 expression in the root tip of *CKX3* mutant. (a) Confocal images of *DR5rev:3xVENUS-N7* signal in the root tips of 4-day-old NIP and *ckx3-1* seedlings grown under LN and HN conditions, in the presence and absence of 10 nM 6-BA or iP for another 1 day. Yellow and red triangles indicate the root epidermis and the stele, respectively. Scale bar, 100 μm. (b) Quantification of *DR5rev:3xVENUS-N7* signaling in root epidermis and stele of the indicated seedlings showing in (a). LN, 0.125 mM $(NH_4)_2SO_4$; HN, 1.25 mM $(NH_4)_2SO_4$. Data are means ± SD (n = 10 individual seedlings). Different lowercase letters above columns indicate significant differences ($P < 0.05$, ANOVA followed by Tukey test).

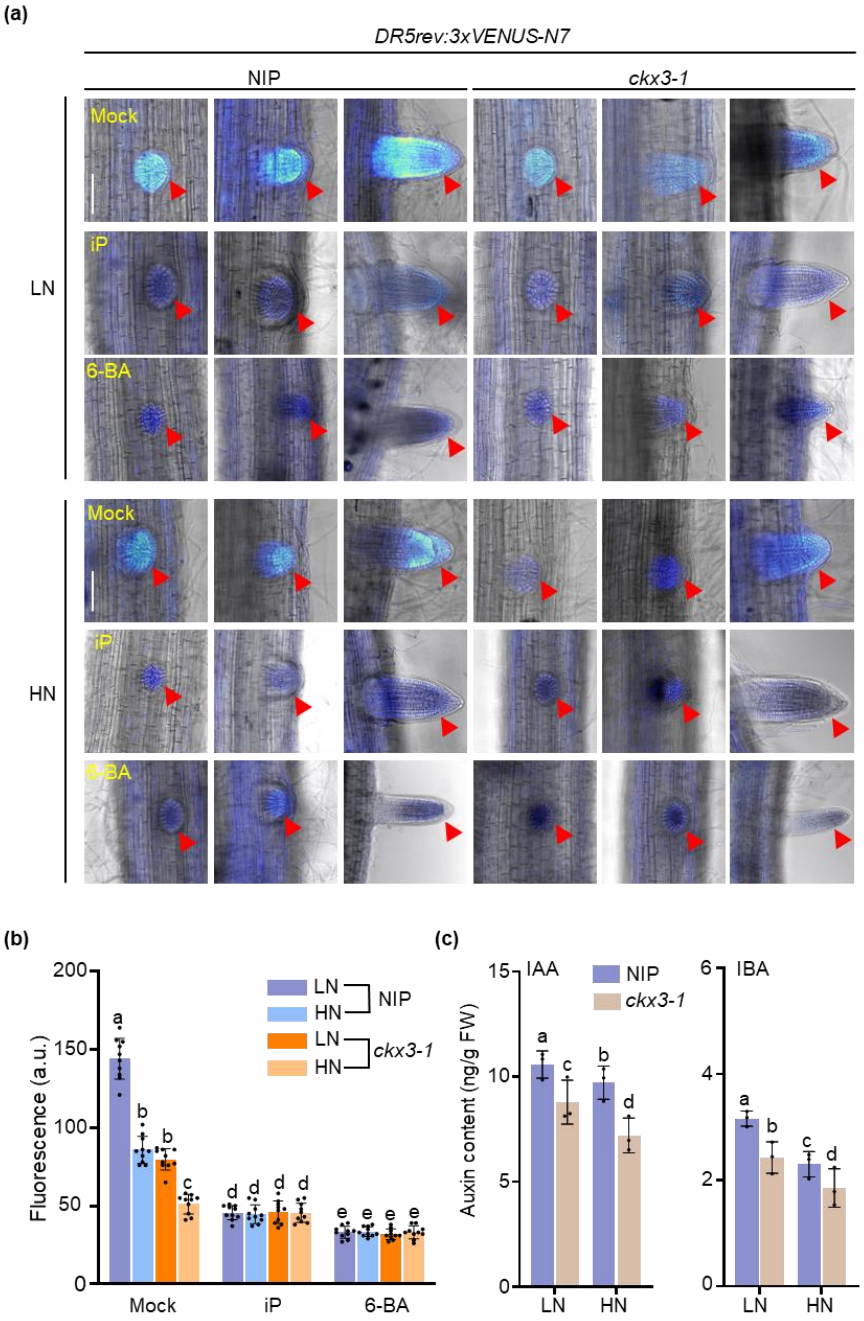

Fig. 10 The effects of NH_4^+ and exogenous cytokinins on the DR5 expression in the lateral root primordia of *CKX3* mutant. (a) Confocal images of *DR5rev:3xVENUS-N7* signal in the lateral root primordia of 4-day-old NIP and *ckx3-1* seedlings grown under LN and HN conditions, in the presence and absence of 10 nM 6-BA or iP for another 1 day. Red triangles indicate the position of lateral root primordia. Scale bar, 100 μm. (b) Quantification of *DR5rev:3xVENUS-N7* signaling in the lateral root primordia of indicated seedlings showing in (a) (n = 10 biological replicates). (c) Quantification of the content of IAA and IBA in the roots of germinated NIP and *ckx3-1* seeds grown under LN and HN conditions for another 7 days (n = 3 biological replicates). LN, 0.125 mM $(NH_4)_2SO_4$; HN, 1.25 mM $(NH_4)_2SO_4$. Data are means

± SD. Different lowercase letters above columns indicate significant differences ($P < 0.05$, ANOVA followed by Tukey test).

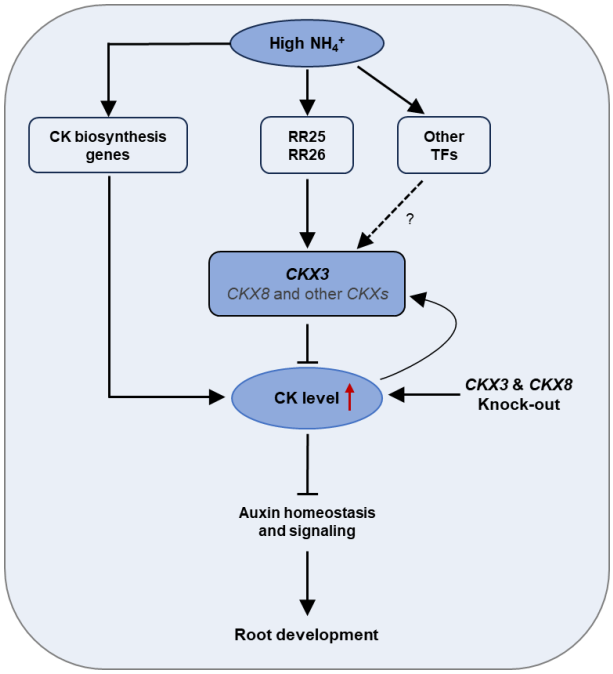

Fig. 11 A working model for CKX3-mediated root growth responses to external high NH_4^+ supply. CK accumulation causes inhibition on auxin signaling/homeostasis and root development; CKXs act on the degradation of endogenous CKs, and play critical roles in regulating endogenous CK levels. In this model, the expression of CK biosynthesis pathway genes are induced by high NH_4^+, accompanied with increased level of endogenous CK derivates, which led to shorter seminal root elongation and higher lateral root density. The *CKX3* and its homologue *CKX8*, are transcriptional activated by B-type RR RR25 and RR26 under high NH_4^+ to reduce endogenous CK levels, in turn attenuating the effects of NH_4^+ on root growth. While the knock-out mutants of *CKX3* and *CKX8* has reduced seminal root elongation and lateral root formation under either high or low NH_4^+ condition, due to the accumulation of CKs *in vivo*, thus exhibiting reduced root sensitivity to high NH_4^+. Furthermore, CKX3 can also be targeted and regulated by other NH_4^+-responsive transcription factors (TFs), and other CKX family members may also play roles in regulating root responses to external NH_4^+.